STABILITY OF RECTILINEAR GEOSTROPHIC VORTICES IN STATIONARY EQUILIBRIUM

Louis Bauer, et al

New York University

Prepared for:

Air Force Office of Scientific Research
Advanced Research Projects Agency

April 1975

IMM 406
April 1975

Courant Institute of

Mathematical Sciences

Stability of Rectilinear Geostrophic Vortices in Stationary Equilibrium

Louis Bauer and George K. Morikawa

Sponsored by Advanced Research Projects Agency,
ARPA Order No. 2774.

New York University

UNCLASSIFIED

SECURITY CLASSIFICATION OF THIS PAGE (When Date Entered)

REPORT DOCUMENTATION PAGE		READ INSTRUCTIONS BEFORE COMPLETING FORM
1. REPORT NUMBER AFOSR - TR - 75 - 1154	2. GOVT ACCESSION NO.	3. RECIPIENT'S CATALOG NUMBER AD-A013839
4. TITLE (and Subtitle) STABILITY OF RECTILINEAR GEOSTROPHIC VORTICES IN STATIONARY EQUILIBRIUM		5. TYPE OF REPORT & PERIOD COVERED Technical 6. PERFORMING ORG. REPORT NUMBER
7. AUTHOR(s) Louis Bauer and George K. Morikawa.		8. CONTRACT OR GRANT NUMBER(s) AFOSR 74-2728
9. PERFORMING ORGANIZATION NAME AND ADDRESS Courant Institute of Mathematical Sciences New York University 251 Mercer St., New York, N.Y. 10012		10. PROGRAM ELEMENT, PROJECT, TASK AREA & WORK UNIT NUMBERS ARPA Order 2774
11. CONTROLLING OFFICE NAME AND ADDRESS Advanced Research Projects Agency 1400 Wilson Boulevard Arlington, Virginia 22209		12. REPORT DATE April 1975 13. NUMBER OF PAGES 70
14. MONITORING AGENCY NAME & ADDRESS(if different from Controlling Office) Air Force Office of Scientific Research/NP 1400 Wilson Boulevard Arlington, Virginia 22209		15. SECURITY CLASS. (of this report) not classified 15a. DECLASSIFICATION/DOWNGRADING SCHEDULE none

16. DISTRIBUTION STATEMENT (of this Report)

Distribution of this document is unlimited.

17. DISTRIBUTION STATEMENT (of the abstract entered in Block 20, if different from Report)

none

18. SUPPLEMENTARY NOTES

none

19. KEY WORDS (Continue on reverse side if necessary and identify by block number)

none

20. ABSTRACT (Continue on reverse side if necessary and identify by block number)

A hemispherical barotropic model of global-scale atmospheric motions is studied in a planar approximation using three K_0 (Bessel)-vortices of equal strength γ and length scale κ^{-1} to represent the sub-tropical semi-permanent high pressure systems. In equilibrium these anticyclonic vortices are equally spaced on

DD FORM 1 JAN 73 1473 EDITION OF 1 NOV 65 IS OBSOLETE

UNCLASSIFIED

SECURITY CLASSIFICATION OF THIS PAGE (When Date Entered)

20. continued:

a latitude circle of radius a. One K_o-vortex of strength γ_o is used to simulate the polar (cyclonic) vortex; γ_o is chosen so that the equilibrium configuration remains stationary with respect to the rotating earth. Over the range of the length parameter $0 \leq (\kappa a) \leq 5$, two distinct stable regimes are found: 1) a "soft"-vortex regime, $0 \leq (\kappa a) < (\kappa_{cr} \cdot a) = 1.44763516$ and 2) a "hard"-vortex (climatological) regime, $\kappa > \kappa_{cr}$. The nonlinear part of this stability investigation has been carried out mainly by numerical computation.

ARPA Order No.: 2774

IMM 406
April 1975

New York University

Courant Institute of Mathematical Sciences

STABILITY OF RECTILINEAR GEOSTROPHIC VORTICES IN STATIONARY EQUILIBRIUM

Louis Bauer and George K. Morikawa

This research was supported by the Advanced Research Projects Agency of the Department of Defense and was monitored by the Air Force Office of Scientific Research under Contract No. AFOSR 74-2728.

Stability of Rectilinear Geostrophic Vortices in Stationary Equilibrium

by

Louis Bauer and George K. Morikawa

Courant Institute of Mathematical Sciences
New York University, New York, N. Y. 10012

Abstract

A hemispherical barotropic model of global-scale atmospheric motions is studied in a planar approximation using three K_o (Bessel)-vortices of equal strength γ and length scale κ^{-1} to represent the sub-tropical semi-permanent high pressure systems. In equilibrium these anticyclonic vortices are equally spaced on a latitude circle of radius a. One K_o-vortex of strength γ_o is used to simulate the polar (cyclonic) vortex; γ_o is chosen so that the equilibrium configuration remains stationary with respect to the rotating earth. Over the range of the length parameter $0 \leq (\kappa a) \leq 5$, two distinct stable regimes are found: 1) a "soft"-vortex regime, $0 \leq (\kappa a) < (\kappa_{cr} \cdot a) = 1.44763516$ and 2) a "hard"-vortex (climatological) regime, $\kappa > \kappa_{cr}$. The nonlinear part of this stability investigation has been carried out mainly by numerical computation.

I. Introduction

Rectilinear geostrophic (Bessel) vortices were first used by Stewart [1,2], to study the periodic properties of the motion of the semi-permanent atmospheric pressure systems. He found that the period of these oscillations is of the order of magnitude of years. He represented the subtropical anticyclones by an equilibrium configuration of three vortices of equal strength γ and length scale κ^{-1} spaced equidistantly on a latitude circle of radius a; but this equilibrium has a slow westerly drifting motion. Another equilibrium configuration, which he considered with an additional cyclonic vortex fixed at the pole to counteract the drift, was found to be unstable [2].

In this paper we study the motion of geostrophic vortices about an equilibrium configuration in which the polar (or center) vortex is free to interact with the three anticyclonic vortices. The strength γ_o of the polar vortex is chosen so that the equilibrium configuration is stationary with respect to the rotating earth. The center-vortex length parameter $\kappa_o = \kappa$ is usually taken; but the effect of different $\kappa_o \neq \kappa$ is discussed briefly. We estimate that the climatological range of the dimensionless length parameter to be $2.5 \leq (\kappa a) \leq 5$. The inclusion of a free polar vortex, albeit a rather simplified representation of the totality of vorticity concentrations at the higher latitudes, introduces two additional degrees of freedom, resulting in a physically meaningful model of atmospheric motions on a hemispherical scale. The present study is an outgrowth of the recent work of Morikawa

and Swenson [3] where the possibility of finding stable motions for this stationary equilibrium configuration is indicated. For the nonlinear problem we say that the motion is unstable if the center vortex goes outside of the equilibrium circle. The comprehensive stability investigation carried out in Ref. [3] shows that the usual normal-mode type of linear stability analysis is not sufficient to determine stable, oscillatory motions, especially due to the stationarity condition. The stationarity condition introduces two additional zero eigenvalues which yield algebraic instabilities in addition to two pairs of eigenfrequencies $\pm\Omega_1$ and $\pm\Omega_2$. This implies that the full nonlinear equations must be studied in order to reveal and ascertain the stable motions. Numerical computations are made for this purpose.

The geostrophic vortex representation is a particular aspect of the barotropic model [4] of atmospheric motion. The principal approximations are: 1) heating and dissipation are neglected, 2) hydrostatic balance replaces the vertical momentum equation, 3) geostrophic balance replaces the horizontal momentum equations and 4) the Coriolis parameter is constant, fixed at a particular latitude, for example, at the pole. Our results indicate that, for the very large-scale pressure systems of planetary dimensions, free long-period oscillatory motions are possible.

In addition, a more comprehensive numerical study has been made over the full range of the length parameter, $0 \leq (\kappa a) \leq 5$. A remarkable phenomenon is found with respect to nonlinear stability over this range of (κa). Normalizing by setting $a = 1$, the stable ranges of κ are divided into two parts: 1) a low κ range,

$0 \leq \kappa < 1.4476$ and 2) a high κ range, $\kappa > 1.4476$ (including the climatological range). The approximate value $\kappa = 1.4476$ corresponds precisely to the frequency ratio $\Omega_2/\Omega_1 = 2$, at which value the motion is unstable for any initial perturbation. Both stable ranges are of physical interest. A comparison of the behavior of the stable nonlinear interacting motions in the two stable regimes shows that the low κ vortices act like "soft" vortices and the high κ vortices act like relatively "hard" vortices. The low κ vortices, especially for $\kappa << 1$, are exceptionally stable for a circle-vortex initial displacement; whereas the hard vortices in the upper climatological regime, e.g. $\kappa = 5$, are very stable for center-vortex initial displacements.

II. Equations of Motion and Condition for Stationary Equilibrium

We study the interacting motion of geostrophic vortices where, initially, the vortices are positioned near a stationary equilibrium configuration which consists of N (anticyclonic) vortices of equal strength γ equally spaced on a (latitude) circle of radius a, and one (cyclonic) vortex of strength γ_o at the center (north or south pole) of the circle; the configuration (with N = 3) which we study is shown in Fig. 1. A single vortex is given by the streamfunction

$$\psi = \gamma K_o(\kappa r) , \quad r = (x^2 + y^2)^{1/2} \tag{1}$$

where positive γ corresponds to anticyclonic (clockwise) motion and K_o is the modified Bessel function of the second kind (zeroth order). The velocity components are

$$(u,v) = (-\frac{\partial \psi}{\partial y} , \frac{\partial \psi}{\partial x}) \tag{2}$$

which also correspond to the conditions for geostrophic motion. The 2(N+1) kinematic equations of motion [3] for interacting geostrophic vortices in Cartesian coordinates are (for k = 1,2,...,N)

$$\dot{x}_k = \kappa^2 \sum_{i \neq k, i=1}^{N} (y_k - y_i) \frac{K_1(\rho_{ki})}{\rho_{ki}} + \gamma_o \kappa^2 (y_k - y_o) \frac{K_1(\rho_{ko})}{\rho_{ko}} \tag{3}$$

$$\dot{y}_k = -\kappa^2 \sum_{i \neq k, i=1}^{N} (x_k - x_i) \frac{K_1(\rho_{ki})}{\rho_{ki}} - \gamma_o \kappa^2 (x_k - x_o) \frac{K_1(\rho_{ko})}{\rho_{ko}} \tag{4}$$

$$\dot{x}_o = \kappa^2 \sum_{i=1}^{N} (y_o - y_i) \frac{K_1(\rho_{oi})}{\rho_{oi}} \tag{5}$$

$$\dot{y}_o = -\kappa^2 \sum_{i=1}^{N} (x_o - x_i) \frac{K_1(\rho_{oi})}{\rho_{oi}} \tag{6}$$

where the dot means time derivative; K_1 is the Bessel function of the second kind (first order); and

$$\rho_{ki} = \kappa[(x_k - x_i)^2 + (y_k - y_i)^2]^{1/2}$$

$$\rho_{ko} = \kappa[(x_k - x_o)^2 + (y_k - y_o)^2]^{1/2}$$

$$\rho_{oi} = \kappa[(x_o - x_i)^2 + (y_o - y_i)^2]^{1/2}$$

The following dimensional normalizations have been made: Lengths are normalized by the circle radius a; time is normalized by (a^2/γ); and the center vortex strength γ_o is normalized by γ. In most of the work described in this paper, one length scale κ^{-1} is associated with each of the vortices. However we have carried out in addition some calculations with another length scale κ_o^{-1} for the center vortex in order to simulate different values of the Coriolis parameter at the pole than at the latitude circle; for these computations, (3) to (6) are modified by replacing κ by κ_o in those terms having the strength factor γ_o of the center vortex.

The general equilibrium condition [3] is uniform rotation of the circle vortices with angular velocity

$$\Omega = \Omega_o + \gamma_o \omega_o \tag{7a}$$

with

$$\Omega_o = \frac{1}{2} \sum_{i \neq k,\, i=1}^{N} \sigma_{ki} K_1(\sigma_{ki})$$

and

$$\omega_o = \kappa K_1(\kappa)$$

where

$$\sigma_{ki} = \kappa[2(1 - \cos w_{ki})]^{1/2}$$

$$w_{ki} = w_k - w_i = w_k^o - w_i^o = \frac{2\pi}{N}(k-i)$$

The superscript denotes the initial equilibrium position. From (7a) the condition for stationary equilibrium is $\Omega = 0$, or

(7b) $$\gamma_o = -\Omega_o/\omega_o$$

For the nonlinear numerical computations we use one of the integrals [5] of the motion [Ref. 3, Appendix B, Eqn. (B9)]:

(8) $$\sum_{k=0}^{N} \gamma_k r_k^2 = \text{const.}$$

(8) is used to monitor the error accumulation.

III. Linearized Stability Analysis

For $N \geq 3$ the $2(N+1)$ linearized equations of motion (constant coefficients) for the perturbed positions $(r_k^{(1)}, \theta_k^{(1)}; \tilde{x}_o^{(1)}, \tilde{y}_o^{(1)})$ from equilibrium are

$$(9)\quad \dot{r}_k^{(1)} + \sum_{i\neq k,\, i=1}^{N} A_{ki} r_i^{(1)} + \sum_{i\neq k,\, i=1}^{N} B_{ki}(\theta_i^{(1)} - \theta_k^{(1)}) + \gamma_o \omega_o(\tilde{x}_o^{(1)} \sin w_k^o - \tilde{y}_o^{(1)} \cos w_k^o) = 0$$

$$(10)\quad \dot{\theta}_k^{(1)} + (\Omega + C_o + \gamma_o D_o) r_k^{(1)} + \sum_{i\neq k,\, i=1}^{N} C_{ki} r_i^{(1)} + \sum_{i\neq k,\, i=1}^{N} A_{ki}\theta_i^{(1)} - \gamma_o D_o(\tilde{x}_o^{(1)} \cos w_k^o + \tilde{y}_o^{(1)} \sin w_k^o) = 0$$

$$(11)\quad \dot{\tilde{x}}_o^{(1)} + D_o \sum_{i=1}^{N} r_i^{(1)} \sin w_i^o - \omega_o \sum_{i=1}^{N} \theta_i^{(1)} \cos w_i^o - (\Omega + E_o)\tilde{y}_o^{(1)} = 0$$

$$(12)\quad \dot{\tilde{y}}_o^{(1)} - D_o \sum_{i=1}^{N} r_i^{(1)} \cos w_i^o - \omega_o \sum_{i=1}^{N} \theta_i^{(1)} \sin w_k^o + (\Omega + E_o)\tilde{x}_o^{(1)} = 0$$

Where

$$A_{ki} = (-\kappa^2/2) \sin w_{ki} K_o(\sigma_{ki})$$

$$B_{ki} = (\kappa^2/2)\{(1 + \cos w_{ki})K_o(\sigma_{ki}) + [2K_1(\sigma_{ki})/\sigma_{ki}]\}$$

$$C_{ki} = (\kappa^2/2)\{(1 - \cos w_{ki})K_o(\sigma_{ki}) + [2K_1(\sigma_{ki})/\sigma_{ki}]\}$$

$$C_o = (\kappa^2/2) \sum_{i\neq k,\, i=1}^{N} \{(1 - \cos w_{ki})K_o(\sigma_{ki}) - 2 \cos w_{ki}[K_1(\sigma_{ki})/\sigma_{ki}]\}$$

$$\sigma_{ki} = \kappa[2(1 - \cos w_{ki})]^{1/2}, \quad w_{ki} = w_{ki}^o = (2\pi/N)(k-i)$$

$$\omega_o = \kappa K_1(\kappa), \quad D_o = \kappa^2\{K_o(\kappa) + [K_1(\kappa)/\kappa]\}, \quad E_o = (N/2)\kappa^2 K_o(\kappa)$$

The position of a circle vortex $(r_k^{(1)}, \theta_k^{(1)})$ is described in polar coordinates and the position of the center vortex $(\tilde{x}_o^{(1)}, \tilde{y}_o^{(1)})$ is described in a Cartesian frame of reference rotating with the equilibrium angular velocity Ω. For $\Omega = 0$, $(\tilde{x}_o^{(1)}, \tilde{y}_o^{(1)}) = (x_o^{(1)}, y_o^{(1)})$ in the rest frame. For no center vortex $\gamma_o = 0$ $(\Omega \neq 0)$, (9) and (10) reduce to equations equivalent to those studied by Stewart [1]. Since (9) and (12) have constant coefficients, the usual exponential stability analysis is possible as described in Ref. 3. In the remainder of this section we summarize the results of these calculations over the range of physical parameters of interest.

First we review, correct and extend the calculations for Stewart's model [1] with $N = 3$ and $\gamma_o = 0$. With 2N degrees of freedom, there are six eigenfrequencies $\pm\Omega_i$ of which two are zero eigenfrequencies [5]. The non-zero eigenfrequencies Ω_o and Ω_{o1}, where Ω_o is the angular velocity of the equilibrium around the circle, are shown in Table I for $\kappa = 3$, 3.5 and 4. Based on Stewart's estimates this range of κ (or (κa)) corresponds nominally to a latitude range between 35° and 20°. We note that, for $N = 3$ and a 20° latitude circle, the equidistance between anticyclones is about 10,000 km; this is also nominally the distance between pole and equator where the geostrophic concept tends to become inapplicable.

Table I. Non-Dimensional Eigenfrequencies for $(N = 3;\ \gamma_o = 0)$

κ	Ω_o	Ω_{o1}	Ω_{o1}/Ω_o
3	0.01690	0.05711	3.38
3.5	0.00761	0.02899	3.81
4	0.00340	0.01440	4.24

The anticyclonic vortex strength γ is estimated from the tangential velocity relation using (1) and (2)

$$|V(r)| = \gamma\kappa K_1(\kappa r) \tag{13}$$

Following Stewart's estimate, the length scale $\kappa^{-1} = 2000$ km. is assumed; for $r = 2000$ km., the characteristic velocity is estimated to be of the order of 10 meters sec^{-1}; then the strength $\gamma = 2.87 \times 10^6$ km^2 day^{-1}. Now the oscillatory periods t_i corresponding to the non-dimensional frequencies Ω_i are obtained by

$$t_i = 2\pi a^2/\gamma\Omega_i = 8.756(\kappa a)^2/\Omega_i \text{ days cycle}^{-1} \tag{14}$$

where a is the distance between pole and latitude circle. The oscillatory periods t_o and t_{o1} corresponding to Ω_o and Ω_{o1} in Table I are given in Table II.

Table II. Oscillatory Periods for ($N=3$; $\gamma_o = 0$)

(κa)	t_o	t_{o1}
	days (years)	days (years)
3	4665 (12.8)	1380 (3.78)
3.5	14100 (38.6)	3700 (10.1)
4	41200 (113)	9730 (26.7)

For $3 \leq (\kappa a) \leq 4$, the time t_o for an anticyclone to drift once around the latitude circle ranges between 13 and 113 years.

Now we introduce a free cyclonic polar (center) vortex in order to nullify this drifting motion. First we investigate the exponential stability for <u>all</u> N when the stationarity condition

$\Omega = 0$ is imposed. From Ref. 3 we find that a circle vortex is exponentially unstable for ($N \geq 4$; $\Omega = 0$) and any value of $\kappa \geq 0$. This is illustrated in Fig. 2 where the dashed curve for ($N = 4$; $\Omega = 0$) is on the stippled unstable side of the neutral stability curve for $N = 4$. For ($N = 2$; $\Omega = 0$) the center vortex is exponentially unstable as shown in Fig. 2. Only for ($N = 3$; $\Omega = 0$) is the stationary equilibrium curve on the exponentially stable side of the corresponding neutral stability curve. With 2(N+1) degrees of freedom, there are eight eigenfrequencies $\pm\Omega_i$ of which four are zero eigenfrequencies [6]. The non-zero eigenfrequencies Ω_1 and Ω_2 and the value of γ_o from the stationarity condition (18) are shown in Table III for κ = 2.5, 3, 3.5, 4, 4.5, and 5. Here the same length scale κ^{-1} has been associated with both center and circle vortices.

Table III. Non-Dimensional Eigenfrequencies for ($N=3$, $\Omega=0$)

κ	γ_o	Ω_1	Ω_2	Ω_2/Ω_1	Ω_o/Ω_1
2.5	-0.2010	0.1498	0.6619	4.417	0.2478
3	-0.1403	0.07694	0.5057	6.573	0.2197
3.5	-0.09780	0.03837	0.3771	9.829	0.1984
4	-0.06809	0.01872	0.2755	14.72	0.1816
4.5	-0.04737	0.008988	0.1978	22.01	0.1679
5	-0.03294	0.004260	0.1399	32.85	0.1564

The oscillatory periods t_1 and t_2 corresponding to the non-dimensional eigenfrequencies Ω_1 and Ω_2 in Table III are again calculated using (14) in the range $3 \leq (\kappa a) \leq 4$ for κ^{-1} = 2000 km.

But in the extended range $2.5 \leq (\kappa a) \leq 3$, we choose $\kappa^{-1} = 2500$ km and $t_i = 10.945(\kappa a)^2/\Omega_i$; and in the extended range $4 \leq (\kappa a) \leq 5$, we choose $\kappa^{-1} = 1500$ km and $t_i = 6.567(\kappa a)^2/\Omega_i$. Then, for the entire range $2.5 \leq (\kappa a) \leq 5$, the range of the corresponding latitude circles lies between 18° and 36°. These oscillatory periods are given in Table IV.

Table IV. Oscillatory Periods for ($N = 3$; $\Omega = 0$)

(κa)	Lat., Deg.	t_1	t_2
		days (years)	days (years)
$\kappa^{-1} = 2500$ km			
2.5	34°	456 (1.25)	103 (0.283)
3	22°	1280 (3.51)	195 (0.534)
$\kappa^{-1} = 2000$ km			
3	36°	1024 (2.81)	156 (0.427)
3.5	27°	2795 (7.66)	284 (0.779)
4	18°	7484 (20.5)	508 (1.39)
$\kappa^{-1} = 1500$ km			
4	36°	5613 (15.4)	381 (1.04)
4.5	29°	14790 (40.5)	672 (1.84)
5	22°	38540 (106)	1170 (3.21)

Table IV shows that, over the length parameter range $2.5 \leq (\kappa a) \leq 5$, the long period range is 1.25 yrs $\leq t_1 \leq$ 106 yrs and the short

period range is 0.283 yrs $\leq t_2 \leq$ 3.21 yrs. The effect of changing the vortex length scale by 500 km. is indicated for two values of $(\kappa a) = 3$ and 4. For these dynamically balanced vortex motions, shorter periods are associated with vortices having larger length scales (smaller κ).

Since the four zero eigenvalues yield algebraic instabilities proportional to t or t^3, the validity of these linearized calculations for ($N = 3$; $\Omega = 0$) depends on the study of the nonlinear equations (3) to (6) by numerical computation.

IV. Numerical Computation of Nonlinear Motions

A. Type of Initial Perturbations

We follow the procedure established in Ref. 3 and restrict the initial perturbation displacement away from equilibrium to only one vortex, either the center vortex or one of the circle vortices. Specifically, four different types of initial perturbations were considered: (a) Displacement of the center vortex, $x_0^{(1)}(0)$ or $y_0^{(1)}(0)$ and (b) displacement of the 3-rd circle vortex, $x_3^{(1)}(0)$ and/or $y_3^{(1)}(0)$ (see Fig. 1). In this section the superscript (1) notation is used to indicate all perturbation displacements, not necessarily in the linear range, but also in the stable nonlinear range (as in Ref. 3 the perturbation parameter ε has been included in the displacement to simplify the notation). From these single initial perturbations plus symmetry considerations, we are able to construct the range of stable initial displacements for center and circle vortices. In the future it would be of interest to consider combined initial displacements of more than one vortex, as well as random initial perturbations for one run or an ensemble of runs.

B. Stationarity Condition for Finite Initial Perturbations

The condition for stationary equilibrium is given by (8). However for various finite initial perturbations especially for large initial displacements, even though the motion is stable in the exponential sense, there will be an appreciable drifting motion unless γ_0 is changed. We have found that this drift is essentially

a uniform rotating motion and can be eliminated by changing the strength ratio γ_o/γ. Thus this drifting motion, arising from large initial perturbations, may be interpreted as an algebraic instability which is removable by correcting γ_o/γ. Therefore a corrected $\hat{\gamma}_o(\kappa a_i)$ is computed so that the circle vortices remain approximately stationary in the mean, where a_i is the distance between the i-th circle vortex and the center vortex. As a first order correction we compute an average distance $\hat{a}$ by

$$\hat{a} = (1/3) \sum_{i=1}^{3} a_i \tag{15}$$

and

$$\hat{\gamma}_o = -\hat{\Omega}_o(\kappa\hat{a})/\hat{\omega}_o(\kappa\hat{a}) \tag{16}$$

In many cases $\hat{\gamma}_o$ is sufficient to nullify the drifting motion. Although a complete elimination of the drifting motion is possible for all stable cases, we have usually not felt the necessity for making finer corrections. In fact a small drifting motion often allows us to discern the form of the circle vortex trajectories more easily when they do not overlap completely after several periods of motion. Of course, when the center vortex becomes unstable and migrates outside of the circle, the circle vortices undergo a drifting motion with angular velocity of the order of Ω_o.

C. Numerical Methods

Originally a Runge-Kutta [7] method was used to solve the system of eight [2(N+1);N = 3] ordinary differential equations (3) to (6) describing the interacting motion of geostrophic vortices.

This procedure is the following: A basic time interval size h_o is chosen. The integration is performed over each interval with a spacing h_o and $h_1 = h_o/2$. If the maximum relative difference in the two integrations is not less than $\varepsilon << 1$, we halve the time step width again, $h_2 = h_1/2$, etc., and repeat the procedure over the subinterval. When two consecutive integrations agree within ε the integration is carried out over h_o with the required subinterval size. At the next interval h_o the procedure is repeated. We observe (and print out) the actual number of subintervals required at each interval. If the number of subintervals becomes excessive (8 or 16), we reduce the basic interval size h_o and redo the problem. We experimented with values of ε of 10^{-8}, 10^{-7} and 10^{-6}, and found that $\varepsilon = 10^{-6}$ was satisfactory for integrations over 1000 intervals, i.e. the change in the final solution for $\varepsilon = 10^{-6}$ and 10^{-8} did not reach the fourth significant digit in the worst case. It is in fact doubtful whether a much smaller value of ε is advantageous because a large number of subintervals leads to accumulation of round-off errors. The standard total time T for any κ was taken to be $2\pi/\hat{\Omega}_o$ where $\hat{\Omega}_o$ is defined by (16). Usually the 1000 time steps was in the range $\pi/2\hat{\Omega}_o \leq T \leq \pi/\hat{\Omega}_o$.

Eventually when the accuracy of the computations was assured, we used a modified Adams method [8] for our integrations, but without re-subdividing each interval. The results are substantially the same as the ones obtained by the Runge-Kutta method and appreciably faster (about 25 seconds per run on the CDC 6600 instead of 145 seconds).

D. Numerical Results for the Climatological Regime

1. Range of Stable Initial Displacements

In the range of the length parameter, $2.5 \leq \kappa \leq 5$, stable nonlinear motions are found over a wide range of initial perturbation displacements of center or circle vortices. For $\kappa < 2$ ($\Omega_2/\Omega_1 < 3$), the magnitude of stable initial perturbations decreases rapidly and approaches zero as $\kappa \to 1.4476$ ($\Omega_2/\Omega_1 \to 2$). This is illustrated in Fig. 3 for initial radial displacements of a circle vortex and in Fig. 4 for initial displacements of the center vortex. These figures show that a second stable regime exists in the small length-parameter range $0 \leq \kappa < 1.4476$ ($1 \leq n < 2$); this complementary, soft-vortex regime will be described later in Section IV-E. In the climatological hard-vortex regime comparison of Figs. 3 and 4 shows that the stability boundary for center-vortex initial displacements is smooth and monotonic with respect to the length parameter κ (Fig. 4); however, the stability boundary for circle-vortex initial displacements shows some non-monotonic wave-like structures – particularly evident in the range $3 \leq \kappa \leq 3.75$, which is in the middle of the estimated climatological regime. The rib-like lines radiating out of the κ-axis are lines of constant frequency ratio, n ($= n_o = \Omega_2/\Omega_1$ on the κ-axis), and n increases with increasing κ from the value $n_o = 1$ at $\kappa = 0$. A more detailed view of the above wave-like structures is found by looking at the stability boundary in the two-dimensional configuration space of center- and circle-vortex initial displacements for several values of κ. Figure 5 shows

both center- and circle-vortex stability boundaries for $\kappa = 3$, 3.5 and 4; Figs. 6 and 7 show the circle-vortex stability boundaries for $\kappa = 3.2$ and 3.5, respectively; and Fig. 8 shows the center-vortex stability boundary for $\kappa = 4$. As shown in Figs. 5 and 8, all the center-vortex stability boundaries are slightly cusped equilateral triangles with smooth faces directed towards the three circle vortices. The vertices of the center-vortex stability triangle are greater than 0.46 from the center for $\kappa = 5$ (Fig. 4) and still increasing for $\kappa > 5$; from geometrical considerations, an apparent limit is the vertex-center distance < 0.5. In the climatological (hard-vortex) regime the center-vortex stability region is substantially larger than the circle-vortex stability region. In the soft-vortex regime $0 \leq \kappa < 1.4476$, this inequality is reversed. Figure 6 for $\kappa = 3.2$ shows the most irregular structure; in fact there are ragged peninsulas and stability islands; the stability boundary is only approximately symmetrical with respect to the radial line through the equilibrium position — we see no reason to expect exact symmetry. Contour lines of constant n are shown; the line, n = 5, goes through the stability islands. In our rather comprehensive numerical calculations, we may still have missed a few islands. For $\kappa = 3.5$ (Fig. 7) there is only one slender island, paralleling the main stability boundary and lying approximately symmetrical with respect to the radial line through the equilibrium position; the contour line, n = 5, passes through the island and the stability boundary is almost coincident with the contour line, n = 6. Figure 3 and comparison between Figs. 6 and 7 show that the major wave-like break-down of the stability

boundary for large amplitude perturbations of a circle-vortex occurs between the frequency ratio, $5 < n < 6$. Even without additional numerical computations, the structure of these irregular stability boundaries in the three-dimensional parameter space $[\kappa; x_3^{(1)}(0), y_3^{(1)}(0)]$ can be visualized for $3 \leq \kappa \leq 3.75$. For example, as the length parameter is changed from $\kappa = 3.2$ to $\kappa = 3.5$, the small islands in configuration space disappear and the peninsulas shrink into one slender island; for $\kappa > 3.65$, this island disappears. In addition to this major irregularity in the stability boundary for $5 < n < 6$, we find smaller stability-boundary-break-down regions for $8 < n < 9$ and $11 < n < 12$, etc. It is remarkable that this rather symmetrical configuration, with only eight degrees of freedom (four Bessel vortices) and with vortices having smooth, monotonic stream functions and velocity distributions, yields such a variety of structure in its stability characteristics for single-vortex initial displacements.

2. Oscillatory Periods and Trajectories of Nonlinear Motions

The linearized stability analysis described in Section III shows that for $(N = 3, \Omega = 0)$ and $\kappa > 0$ there are two pairs of non-zero eigenfrequencies, Ω_1 and Ω_2 and corresponding periods (cf. Tables III and IV). We now interpret these periods in terms of the vortex trajectories for small initial displacements equal to 0.001 with $\kappa = 2$: In Fig. 9a, $x_3^{(1)}(0) = 0.001$; in Fig. 9b, $x_3^{(1)}(0) = -0.001$; in Fig. 9c, $y_3^{(1)}(0) = 0.001$; and in Fig. 9d, $x_0^{(1)}(0) = 0.001$. These trajectories are enlarged 500 times. The vortex trajectories for negative initial displacements are

obtainable from the vortex trajectories for positive initial displacements by rotating each vortex trajectory about its own equilibrium position by π (or one-half revolution, cf. Figs. 9a and 9b). In each case, the center-vortex trajectory has counterclockwise loops progressing clockwise about the origin with a single excursion taking place after four loops; and subsequently recurrence takes place. In all cases the normalized recurrence time (or period) $\Omega_o/\Omega_R = 0.2864$, which agrees with the linearized long period Ω_o/Ω_1 ($\Omega_o = 0.0803$) for $\kappa = 2$. In the time $t_R = 2\pi/\Omega_R$, each circle vortex makes a counterclockwise excursion around a closed trajectory near its equilibrium position. In the linearized analysis the frequency ratio $n_o = (\Omega_2/\Omega_1) = (t_1/t_2)$; for $\kappa = 2$, $n_o = 3.000$. We define the short period as t_R/n; from the center-vortex trajectory for $\kappa = 2$ with small initial displacement, n is equal to (four counterclockwise loops) minus (one clockwise excursion). Generally n is an integer only for certain discrete values of κ, where n increases for increasing κ. Between two consecutive integer values of n, say n_1 and n_2, there will be two-excursion recurrence for κ corresponding to a frequency ratio $(n_1 + 1/2)$, three-excursion recurrence for κ's corresponding to frequency ratios $(n_1 + 1/3)$ and $(n_1 + 2/3)$, etc.; for irrational values of n there will be no recurrence at all. From the center-vortex trajectory with recurrence, the general algorithm for rational values of n is:

$$n = \frac{[(\text{number of loops}) - (\text{number of excursions in one recurrence})]}{(\text{number of excursions in one recurrence})}$$

This algorithm for determining the frequency ratio n is applicable for all initial displacements with recurrent trajectories in the entire range of stable motions. In the climatological range ($n > 2$) for fixed κ, n decreases monotonically from its linear value as the initial displacement is increased to the stability boundary (see Figs. 3 and 4). The dependence of the normalized recurrence time $\hat{\Omega}_o/\Omega_R$ on n for center- and circle-vortex initial displacements is shown in Fig. 10 for $\kappa = 2.5$, 3, 3.5, 4, 4.5 and 5. For each κ, the upper curve is for negative initial radial displacements of a circle vortex $x_3^{(1)}(0) < 0$, $y_3^{(1)}(0) = 0$ and the lower curve is for negative initial displacements of the center vortex $x_o^{(1)}(0) < 0$, $y_o^{(1)}(0) = 0$. All the curves are apparently linear; and specifically for $x_o^{(1)}(0) < 0$, the short period $t_R/n = \text{const.} = t_2 = t_1/n_o$ with less than 5% deviation. For each κ, the curves for all other types of initial displacements are bracketed by these two curves. The dependence of the vortex-strength ratio $|\hat{\gamma}_o|^{-1}$ on n for center- and circle-vortex initial displacements is shown in Fig. 11 for $\kappa = 2.5$, 3, 3.5, 4 and 5. For each κ, the upper curve is for positive initial radial displacements of a circle vortex $x_3^{(1)}(0) > 0$ and the lower curve is for negative initial radial displacements $x_3^{(1)}(0) < 0$. The curves for all other initial displacements are bracketed by these two curves, including the curve for negative initial displacements of the center vortex $x_o^{(1)}(0) < 0$ which is shown explicitly. The normalized recurrence times $\hat{t}_R/t_1$ and the vortex-strength ratios $|\hat{\gamma}_o|^{-1}$ for integer values of n near the stability boundary are given in Table V for circle-vortex initial displace-

Table V. Recurrence Times for Circle-Vortex Initial Displacements $x_3^{(1)}(0)$

κ	$[x_3^{(1)}(0), y_3^{(1)}(0)]$	$\lvert\hat{\gamma}_0\rvert^{-1}$	n	$\hat{t}_R/t_1$
2.5	(-0.126, 0)	4.62	3	0.783
2.5	(0.220, 0)	5.68	3	0.795
3	(0.240, 0)	8.47	4	0.763
3.5	(-0.158, 0)	8.95	5	0.699
4	(-0.160, 0)	12.58	7	0.686
4	(0.215, 0)	18.07	10	0.789
4.5	(-0.160, 0)	17.73	11	0.706
5	(-0.165, 0)	24.86	14	0.657
5	(0.216, 0)	39.35	23	0.796

Table VI. Recurrence Times for Center-Vortex Initial Displacements $x_0^{(1)}(0)$

κ	$[x_0^{(1)}(0), y_0^{(1)}(0)]$	$\lvert\hat{\gamma}_0\rvert^{-1}$	n	$\hat{t}_R/t_1$
2.5	(-0.28†, 0)	5.3†	2.5	0.566†
3	(-0.360, 0)	7.74	2.5	0.396
3.5	(-0.400, 0)	11.54	3	0.315
4	(-0.410, 0)	17.00	4	0.276
4.5	(-0.44†, 0)	25†	4	0.182†
5	(-0.450, 0)	38.29	5	0.148

† Estimates from Figs. 4, 10 and 11.

ments $x_3^{(1)}(0)$ and in Table VI for center-vortex initial displacements $x_o^{(1)}(0)$. The real recurrence times $\hat{t}_R$ can be calculated from the linearized values of the long period t_1 given in Table IV. For example, for $[\kappa,n;x_o^{(1)}(0),y_o^{(1)}(0)] = (5,5;-0.450,0)$, $\hat{t}_R = 0.15 \times 106$ yrs $= 16$ yrs and the short period $\hat{t}_R/n = 3.2$ yrs $= t_2$.

The center-vortex trajectory for small initial perturbations is confined in a circular annulus, which changes into a triangular annulus for large initial displacements approaching the stability boundary. For both center- and circle-vortex perturbations, the center-vortex-trajectory loops become cusped for large-amplitude motions near instability. When the motion becomes unstable, the center vortex goes outside of the circle. Several typical trajectories are shown in the range $2.5 < \kappa < 5$: Fig. 12 shows the trajectories for a small initial tangential displacement of a circle vortex, $[\kappa,n;x_3^{(1)}(0),y_3^{(1)}(0)] = (2.66,5;0,0.001)$; comparing to Fig. 9, the center-vortex trajectory is seen to loop <u>out</u> for a $y_3^{(1)}(0)$ displacement and loop <u>in</u> for an $x_3^{(1)}(0)$ displacement. Two series of recurrent trajectories near the stability boundary, including unstable trajectories outside the stability boundary, are shown in Figs. 13 and 14 for $\kappa = 3.2$: 1) In Fig. 13a, $[\kappa,n;x_3^{(1)}(0),y_3^{(1)}(0)] = (3.2,6;0.196,0)$ and $\hat{t}_R/t_1 = 0.860$; in Fig. 13b with $[x_3^{(1)}(0),y_3^{(1)}(0)] = (0.215,0)$, the center vortex becomes unstable after approximately four-seventh of the recurrence time for $n = 6$ (cf. Fig. 13a); in Fig. 13c $[\kappa,n;x_3^{(1)}(0),y_3^{(1)}(0)]$ $= (3.2,5;0.230,0)$ and $\hat{t}_R/t_1 = 0.789$ and the initial displacement lies on the stability island on the x-axis in Fig. 6; in Fig. 13d with $[x_3^{(1)}(0),y_3^{(1)}(0)] = (0.240,0)$, the center vortex becomes

unstable after approximately a full recurrence time for n = 5 (cf. Fig. 13c). And 2) in Fig. 14a, $[\kappa,n;x_3^{(1)}(0),y_3^{(1)}(0)]$ = (3.2,5;-0.120,0.208) with $\hat{t}_R/t_1$ = 0.810 wherein the circle-vortex initial displacement has a large tangential component and the initial position lies on the upper peninsula in Fig. 6; in Fig. 14b, $[\kappa,n;x_3^{(1)}(0),y_3^{(1)}(0)]$ = (3.2,9/2;-0.130,0.240) and $\hat{t}_R/t_1$ = 0.787 wherein the initial position lies near the stability boundary on the upper peninsula; in Fig. 14c with $[x_3^{(1)}(0),y_3^{(1)}(0)]$ = (-0.120,0.235), the center vortex becomes unstable after more than two recurrence times for n = 9/2 (cf. Fig. 14b). Comparison of series 1) (Fig. 13) with series 2) (Fig. 14) shows some features in common as well as contrasting or distinguishing characteristics of trajectories for radial vs. predominantly tangential initial displacements. The common features are: the circle vortices make the same number of excursions about their equilibrium positions as the center vortex about the configuration center; usually the stable trajectories are confined within the stability boundaries with the exception of initial displacements on islands or peninsulas; near the stability boundary the center vortex tends to make cusps for any type of large initial displacement; there is bilateral symmetry of the stable configurations (after a recurrence time) with respect to a radial line parallel or nearly parallel to the x-axis; the unstable center vortex first becomes captured by one of the three circle vortices, but then changes partners, progressing in a clockwise order about the center. In the least unstable of the three unstable cases shown for κ = 3.2, the center vortex returns to the center of the

configuration for a brief time (Fig. 14c). The contrasting features are: for radial initial displacements, the center vortex makes inside loops about the center and the circle vortex trajectories tend to loop out or make cusps (Fig. 13); while for predominantly tangential displacements the center vortex makes outside loops (away from the center) and cusps while the circle vortex trajectories are relatively smooth. Next, an example of recurrent trajectories for a center-vortex initial displacement near the stability boundary is shown in Fig. 15 for $[\kappa,n;x_o^{(1)}(0),y_o^{(1)}(0)]$ $= (3.5,4;0.1955,0)$ and $\hat{t}_R/t_1 = 0.508$. The center-vortex trajectory is confined in a narrow annulus so that a second-order drift correction of -11.1% is required in order to resolve the frequency ratio n = 4; also the circle vortex trajectories are difficult to resolve. Finally in Fig. 16 for $[\kappa,n;x_3^{(1)}(0),y_3^{(1)}(0)]$ $= (4.5,15;0.2138,0)$ and $\hat{t}_R/t_1 = 0.785$, an example is shown of recurrent trajectories for a circle-vortex initial displacement near the stability boundary with a relatively large κ and n.

E. Soft Vortices Compared to Hard Vortices

1. Mainly Stable Motions

The behavior of the soft vortices in the small-length-parameter range $0 \leq \kappa < 1.4476$ $(1 \leq n < 2)$ is compared with the characteristics of the hard (climatological) vortices. The variation of the stability boundary with respect to κ for initial radial displacements along the x-axis of a circle vortex and center vortex have already been shown in Figs. 3 and 4 respec-

tively. Comparing the inclination of the n-contours (constant frequency ratio Ω_2/Ω_1) for large displacements in the soft-vortex regime with the slope of the n-contours in the hard-vortex regime, both sets of contours are directed away from the instability point, $\kappa_{cr} = 1.4476$ (n = 2) for increasing values of the initial displacements. The numerical calculations show that in the range $1 < \kappa < 2$, which straddles the instability point, the stability boundary itself approximates a node-like contour, n = 2; this is most evident for negative initial radial displacement of a circle vortex (or a positive initial displacement of the center vortex) on the soft-vortex side of κ_{cr} and for positive initial radial displacement of a circle vortex (or a negative initial displacement of the center vortex) on the hard-vortex side of κ_{cr}; see Fig. 17 for $[\kappa,n;x_3^{(1)}(0),y_3^{(1)}(0)] = (1.25,2;-0.118,0)$ with $\hat{t}_R/t_1 = 0.6175$ and a second-order drift correction (approximately -1%) was not made; when a drift correction is incorporated into the run shown in Fig. 17, this run is clearly shown to be unstable, i.e. any run with n = 2 is unstable. Figure 3 shows that with a circle-vortex initial displacement for small κ (or n approximately equal to one) the soft-vortex configuration is appreciably more stable than the hard vortex configuration (with n > 2). In contrast Fig. 4 shows that, with a center-vortex initial displacement, the soft-vortex configuration is less stable than the hard-vortex configuration. In Fig. 18 the stability boundaries are shown in the two-dimensional configuration space and center- and circle-vortex initial displacements for $\kappa = 0.75$; the vertices of the triangle-like stability boundaries are directed toward each

other. In contrast the "vertices" of the stability boundaries for center- and circle-vortex initial displacements in the hard-vortex regime shown in Fig. 5 are directed away from each other.

The dependence of the normalized recurrence time $\hat{\Omega}_o/\Omega_R$ on the frequency ratio n for some center- and circle-vortex initial displacements is shown in Fig. 19 for soft vortices κ = 0, 0.25, 0.50, 0.75, 1.0 and 1.25. For each κ the upper curve is for positive initial radial displacements of a circle vortex $x_3^{(1)}(0) > 0$, $y_3^{(1)}(0) = 0$; and the lower curve, which first dips below the linear curve, is for negative initial radial displacements of a circle vortex $x_3^{(1)}(0) < 0$, $y_3^{(1)}(0) = 0$. The curves for all other initial displacements lie between these two curves, including the single curve for all (±) center-vortex initial displacements which is shown explicitly for two κ's, κ = 0.75 and 1.0. In contrast the corresponding hard-vortex curves all lie below the linear curve (see Fig. 10).

The dependence of the vortex-strength-ratio $|\hat{\gamma}_o|^{-1}$ on the frequency ratio n for circle-vortex initial displacements is shown in Fig. 20 for κ = 0, 0.25, 0.50, 0.75 and 1.0. For each κ, the upper curve is for positive initial radial displacement of a circle vortex $x_3^{(1)}(0) > 0$, $y_3^{(1)}(0) = 0$; and for κ = 0.75 and 1.0 the lower curve is for negative initial radial displacement of a circle vortex $x_3^{(1)}(0) < 0$, $y_3^{(1)}(0) = 0$. Curves for other initial displacements are bracketed by these curves which have a small spread in the soft-vortex regime. In contrast the corresponding hard-vortex curves all lie above the linear curve (see Fig. 11). Note that the coordinates are much enlarged in Fig. 20 as compared to Fig. 11.

A number of recurrent trajectories of soft-vortex motion are shown next, mainly near the stability boundary. In addition 1) for $\kappa = 0.125$, a run is shown without a second-order drift correction to compare with the corresponding compensated recurrent trajectories without the drifting motion; and 2) for $\kappa = 0$ the small initial perturbation runs are shown as well as two unstable runs beyond the stability boundary. A comprehensive series of recurrent trajectories for initial radial displacements of a circle vortex for $\kappa = 0.75$, 0.50, 0.25, 0.125 and 0 follows: In Fig. 21, $[\kappa,n;\ x_3^{(1)}(0),y_3^{(1)}(0)] = (0.75,3/2;-0.350,0)$ and $\hat{t}_R/t_1 = 1.06$ with a -5% second-order drift correction; the center-vortex trajectory (and envelope) is reminiscent of a large center-vortex initial displacement in the hard-vortex regime (cf. Fig. 15); in fact the motion of the center vortex is outside of the center stability boundary shown in Fig. 18, albeit for relatively short periods of time; this behavior differs from the hard-vortex regime where the center-vortex trajectory is always confined by the stability boundary. In Fig. 22, $[\kappa,n;x_3^{(1)}(0),y_3^{(1)}(0)] = (0.5,5/4;0.264,0)$ and $\hat{t}_R/t_1 = 1.25$ with a -1.5% second-order drift correction; for positive initial radial displacements the vortex trajectories are confined within their respective stability boundaries; and each vortex makes four excursions around its equilibrium position. Two neighboring recurrent trajectories are shown for $\kappa = 0.25$: In Fig. 23a, $[\kappa,n;x_3^{(1)}(0),y_3^{(1)}(0)] = (0.25,25/19;0.452,0)$ and $\hat{t}_R/t_1 = 1.58$ with a -3.2% second-order drift correction and 19 excursions in a recurrence time; in Fig. 23b, $[\kappa,n;x_3^{(1)}(0),y_3^{(1)}(0)] = (0.25,4/3;0.456,0)$ and $\hat{t}_R/t_1 = 1.61$ with a -3.3% second-order

drift correction and only three excursions in a recurrence time; the difference in the initial displacement is just 0.004 and the difference in the frequency ratio $\Delta n = 1/57$ between the two runs; this is the best resolution we have made of neighboring frequency ratios. In Fig. 24a, $[\kappa, n; x_3^{(1)}(0), y_3^{(1)}(0)] = (0.125, 27/26; 0.250, 0)$ and $\hat{t}_R/t_1 = 1.20$ with a -1.15% second-order drift correction and 26 excursions in one recurrence time; without this small second-order correction, a considerable drifting motion occurs as shown in Fig. 24b. Three recurrent trajectories are shown for $\kappa = 0$: In Fig. 25a,b,c,d $(\kappa, n) = (0, 1)$ with 0.001 initial perturbation for a) $x_3^{(1)}(0)$, b) $y_3^{(1)}(0)$, c) $x_o^{(1)}(0)$ and d) $y_o^{(1)}(0)$; negative-perturbation trajectories are obtained by rotating the positive-perturbation trajectories by π around the equilibrium position for each of the vortices; the initially displaced center-vortex motion is a linear oscillation (Fig. 25c,d); in Fig. 26a, $[\kappa, n; x_3^{(1)}(0), y_3^{(1)}(0)] = (0, 8/7; 0.503, 0)$ and $\hat{t}_R/t_1 = 1.53$ with a -3.55% second-order drift correction and seven excursions in one recurrence time; in Fig. 26b, $[\kappa, n; x_o^{(1)}(0), y_o^{(1)}(0)]$ $= (0, 6/5; 0.300, 0)$ and $\hat{t}_R/t_1 = 1.09$ with a -2% second-order drift correction; in all these cases the trajectories are confined within their stability boundaries. Finally two unstable trajectories are shown for $\kappa = 0$: In Fig. 27a, $[x_o^{(1)}(0), y_o^{(1)}(0)]$ $= (-0.300, 0)$ with $\gamma_o = -1.0$ and no drift correction whatsoever in which case the center-vortex is absolutely unstable and goes to infinity with one of the circle vortices while the remaining two vortices are left to themselves in a circular trajectory; in Fig. 27b, $[x_3^{(1)}(0), y_3^{(1)}(0)] = (0.600, 0)$ and $\hat{\gamma}_o = -0.93500$ with a

-6.5% second-order drift correction; in contrast to the run without a drift correction, the center-vortex is soon captured by one of the circle vortices for a nearly circular excursion far outside the original circle, then goes on to a second trip with the next circle vortex, progressing in a counter-clockwise order.

2. The Instability or Critical Point, $\kappa_{cr} = 1.44763516$ (n = 2)

The problem of determining by numerical calculation that this (3+1)-vortex configuration is unstable at κ_{cr} is not easy since the configuration apparently tends toward stability in an algebraic manner as the initial perturbation is decreased toward zero; in this particular circumstance, a second-order analytical calculation is being carried out, which may turn out to be easier and will verify our present results. In the following sequence of runs we find that certain types of equal-amplitude initial displacements are more stable than others; this structural feature compounds the numerical difficulties. In Fig. 28a,b,c,d,e the initial displacements are a) $x_3^{(1)}(0) = -0.005$, b) $y_3^{(1)}(0) = 0.005$, c) $y_3^{(1)}(0) = -0.005$, d) $x_0^{(1)}(0) = 0.005$ and e) $y_0^{(1)}(0) = 0.005$; all other component displacements are in their equilibrium positions in all of these figures. Only in Fig. 28e is instability an uncertainty and those initial displacements not shown, viz. $x_3^{(1)}(0) = 0.005$ and $x_0^{(1)}(0) = -0.005$, are just as unstable as those of opposite sign (cf. Figs. 28a and 28d). Thus in Fig. 29a,b are shown the trajectories for a) $y_0^{(1)}(0) = 0.015$ and b) $y_0^{(1)}(0) = 0.02$; the center-vortex trajectory in Fig. 29b is

clearly becoming unstable. Finally in Fig. 30a,b for a) $[x_o^{(1)}(0), y_o^{(1)}(0)] = (0.01, 0.03)$ and b) $[x_o^{(1)}(0), y_o^{(1)}(0)] = (-0.01, 0.03)$, the center vortex goes outside of the circle and is captured by one or more circle vortices in sequence.

3. Unstable Motions

Our study of unstable motions is limited in scope because of our self-imposed restriction to emphasize those motions in which the center (cyclonic) vortex remains inside the circle of anti-cyclonic vortices and where the vortex-strength ratio $\hat{\gamma}_o$ is such that the stationarity condition holds. These motions are unstable only in the sense that the trajectories do not remain in the immediate neighborhood of the stationary equilibrium positions for each of the four vortices; this is a necessary condition from the viewpoint of the climatological problem but possibly not for other physical applications of these hard and soft vortices. Otherwise we could regard these motions as not unstable but as a change in mode from motions near one equilibrium state into some other quasi-equilibrium motions. Here we show two more examples of unstable motions and a summarizing result concerning the strength of the nonlinear interaction between vortex pairs moving in the second mode of quasi-periodic motions; these results include many runs (more than 600 or approximately 10% of the total number of runs) over the entire range of the length parameter $0 \leq \kappa \leq 5$. In Fig. 31 unstable trajectories are shown for $\kappa = 5$ and $[x_o^{(1)}(0), y_o^{(1)}(0)] = (0.210, 0)$; the order of capture of the center

vortex by one of the circle vortices is 2-3-1-3-2-1-3 which shows that, after the first two irregular transfers the capture-ordering appears to progress in a regular (hard-vortex) clockwise direction; and the center and circle vortices progress in a clockwise direction with nearly circular loops in phase with each other during the time of capture. In Fig. 32 unstable trajectories are shown for $\kappa = 2.5$ and $[x_3^{(1)}(0), y_3^{(1)}(0)] = (-0.130, 0)$; here the circle vortex is captured for three transits by the #1 circle vortex.

In the case of climatological instability the vortex, originally at the center of the circle, leaves the vicinity and follows a path going around first one of the circle vortices, then another one, etc. Because of the nonlinearity of the problem it is virtually impossible to predict in what order the "center" vortex will be captured by the circle vortices. Certain generalized observations about these trajectories can nevertheless be made: When the motion is still in or near the region of stability, the center vortex will spend some time – several loops – near the center. Then it takes off suddenly (exponentially), encircles one of the circle vortices, and returns to the center, only to take off again later on. In this case the order in which the circle vortices are taken up is completely unpredictable numerically. Farther out in the region of instability, the center vortex takes off almost immediately, and after circling one of the circle vortices, takes up another one, etc., often in a systematic order. Very occasionally it will circle one of the outer vortices twice or more times in succession. For soft vortices there also exists

the possibility of total capture by only one circle vortex, i.e. the center vortex encircles one of the circle vortices almost indefinitely, while the remaining two vortices circle each other.

The radii of the approximate circles formed by the trajectories appear to be of some significance, and bear some relationship to the value of the vortex strength ratio $\hat{\gamma}_o$. In order to make a good numerical approximation to the radii of these circles, the numerical results were analyzed as follows: Whenever the coordinates of the "center" vortex become such that $x^2 + y^2 > 1$, i.e. whenever that vortex left the interior of the unit circle, the coordinates at all succeeding time intervals were stored in the computor memory until the vortex returned to the interior of the circle. The coordinates so obtained were fitted by a least-square procedure into a circle, and the center and radius of that circle computed. The same calculation was done at the same time for the coordinates of the circle vortices. An inspection of the results for the four vortices made it a simple matter to decide which two had a common center (one vortex going in phase around the other). The radii of these two vortices were then determined, and the ratio of these radii were found to be closely correlated to $|\hat{\gamma}_o|^{-1}$. In fact in the absence of the other two vortices, this Radii Ratio is equal to the inverse ratio of the vortex strengths. In Fig. 33 the variation of $|\hat{\gamma}_o| \cdot$(Radii Ratio) with respect to κ is shown for $0 \leq \kappa \leq 5$: 1) it is nominally equal to one for $\kappa = 0$; 2) it decreases to a minimum value equal to 0.7 at $\kappa = 4$; and 3) it apparently increases for $\kappa > 4$ (this increase may be attributable to numerical inaccuracies for $(\kappa r) \geq 10$).

In Ref. 3, Appendix B the sum $\Sigma \equiv \sum_{k=0}^{N} \gamma_k r_k^2 \dot{\theta}_k$ has been shown to be constant for 1) $\kappa = 0$ and 2) after linearization; we have pointed out in Footnote 5 that Σ is usually not an invariant for $\kappa > 0$. This sum may be useful for studying the unstable motions, as well as for future studies of the statistical properties of Bessel vortices. Compared to logarithmic vortices ($\kappa = 0$), these Bessel vortices have better physical properties: 1) finite kinetic energy and 2) one less integral constraint.

V. Remarks

A. An Interpretation of Soft and Hard Vortex Stability

In Ref. 3 the applicability of the study of kinematic (quasi-dynamically-balanced, time-asymptotic) motion to a large range of length scales in suitable physical problems has been pointed out. Our present study supports this viewpoint for at least two different length (and time) scales of atmospheric motions: 1) In Ref. 9 our barotropic model has been applied to the tracking of hurricane motion, using one Bessel vortex, where the normalized length parameter κ was chosen in the range $1 \leq \kappa \leq 4/3$; this κ-range in our present context is in the soft-vortex regime; while 2) our (3+1)-vortex representation of global-scale hemispherical motions is in the hard-vortex regime. One possible interpretation of our stability results, showing the existence of two distinct stable regimes separated by a critical instability point κ_{cr} (with $n = \Omega_2/\Omega_1 = 2$), is that there is a short-range moderate-scale atmospheric description available as well as a longer-range global-scale, kinematic representation; but an intermediate-scale regime of relatively disordered motions exists where some statistical information may be necessary. This conforms to our qualitative observations of natural phenomena in which there is a sequence of ordered and disordered motions depending on different length and time scales. For the short-range description of atmospheric motions, there is apparently an upper limit of about three or four weeks to the predictability of the physical variables using a kinematical (or dynamical) model; and the use of combined kinematical-statistical model has been studied recently by a number of atmospheric scientists, e.g. Leith [10].

B. Applicability of the (3+1)-Vortex Configuration to Climatology

It may seem surprising that this simple configuration of four K_o-vortices can be at all representative of atmospheric motions. Nevertheless our present study shows the apparent validity of this planar model in simulating some basic properties of global-scale motions with correspondingly long time-scales greater than a season, a year or tens of years. One factor which gives us some confidence in the reality of this lowest order barotropic model is that, in the climatological range of the length parameter, the vortex strength ratio is small (less than 0.2).

A few runs were made to estimate the effect of the variation of the Coriolis parameter between the anticyclonic latitude circle and the pole. Both κ (circle vortex) and κ_o (center vortex) were varied in the range $2 \leq (\kappa;\kappa_o) \leq 4$. We find that the value of κ essentially controls the stability properties over a wide range of values of κ_o. For example comparing $(\kappa;\kappa_o) = (4;2)$ with $\kappa = \kappa_o = 4$, the stability boundaries for circle- or center-vortex initial displacements differ by less than 0.01.

The extension of this approach toward more realistic geometry and configurations is being pursued. Peters [11], and Leiva [12] have recently begun the study of vortex motions on a rotating sphere. Leiva's dissertation shows some of the quantitative connections between the linearized stability analysis on the sphere as compared to the planar approximation; the qualitative relationships are quite similar; however a more complete study of the nonlinear motions is required.

References

1. H. J. Stewart, Quart. Appl. Math. 1, 262 (1943).

2. _____, Bull. Am. Math. Soc. 51, 781 (1945).

3. G. K. Morikawa and E. V. Swenson, Phys. Fluids, 14, 1058 (1971).

4. _____, J. Meteorol. 17, 148 (1960).

5. As a correction we find that the sum $\sum_{k=1}^{N} \gamma_k r_k^2 \dot{\theta}_k$ in Ref. 3, Appendix B, Eqn. (B10), is generally not an invariant for $\kappa > 0$; but linearization leads to $\sum_{k=1}^{N} \gamma_k \theta_k = \text{const.} \neq 0$.

6. Without the stationarity constraint (7b) there are only two zero eigenfrequencies for all values of γ_o and κ. As shown in Ref. 3, for $\gamma_o \neq 0$ these zero eigenfrequencies can already lead to algebraic instabilities.

7. L. Bauer, E. Reiss and H. B. Keller, Comm. Pure Appl. Math., 23, p. 538 (1970).

8. E. Isaacson and H. B. Keller, Analysis of Numerical Methods, John Wiley, New York, p. 388 (1966). (Improved Adams' or Moulton's Method.)

9. G. K. Morikawa, Proceedings of Intern. Symp. on Numerical Weather Prediction, Tokyo, Nov. 7-13, 1960, Meteorol. Soc. of Japan (1962), pp. 349-60.

10. C. E. Leith, Proceedings of Intern. Symp. on Spectral Methods in Numerical Weather Prediction, Copenhagen, 12-16 Aug. 1974, to be published.

11. A. Peters, Geostrophic Vortices on a Circle in a Cap on a Rotating Sphere, NYU Report IMM 404 (July, 1974).

12. C. A. Leiva, Stability of Geostrophic Vortices on a Sphere, NYU Report IMM 405 (Dec. 1974).

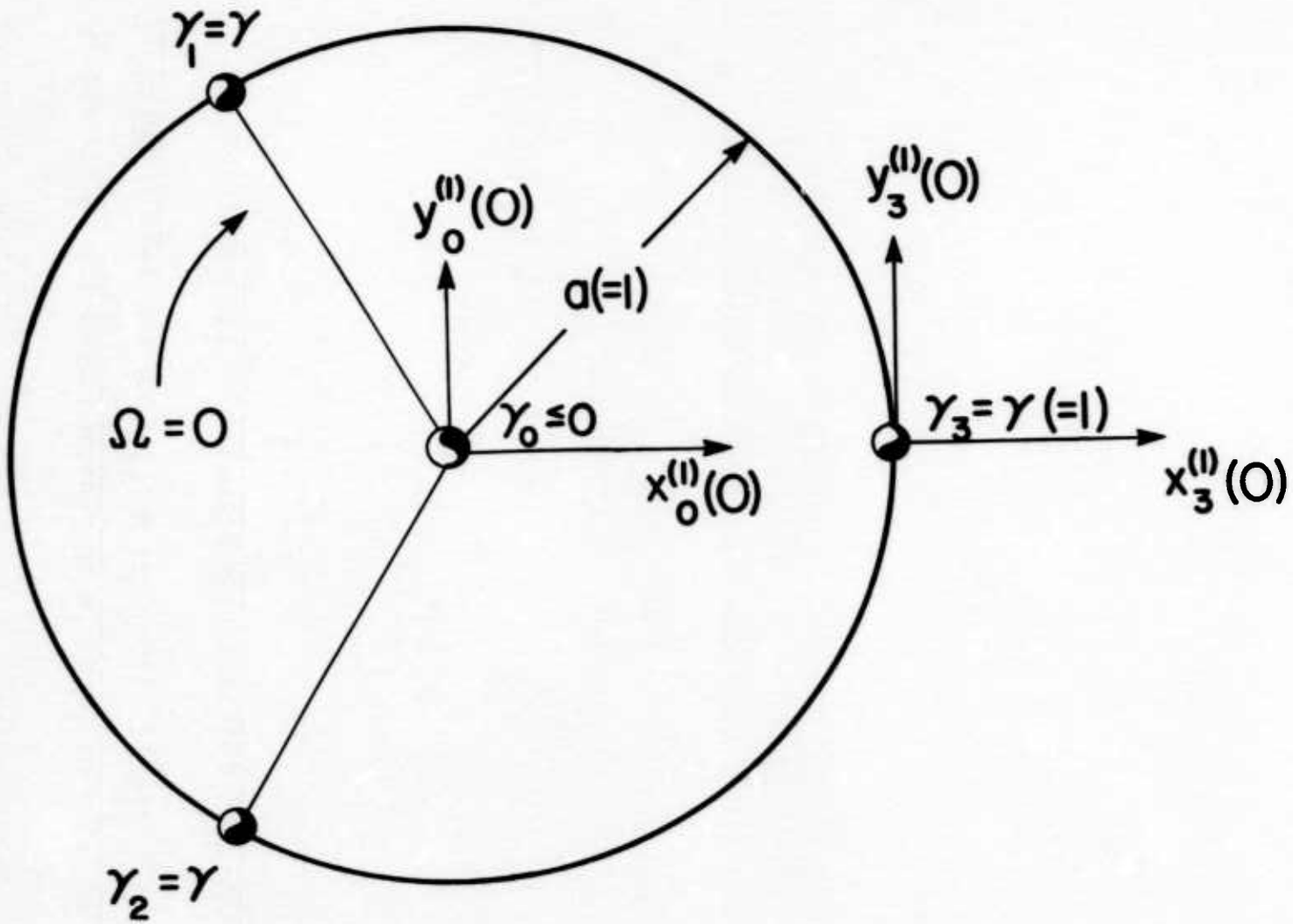

Fig. 1 Equilibrium Configuration for $(N=3;\Omega=0)$.

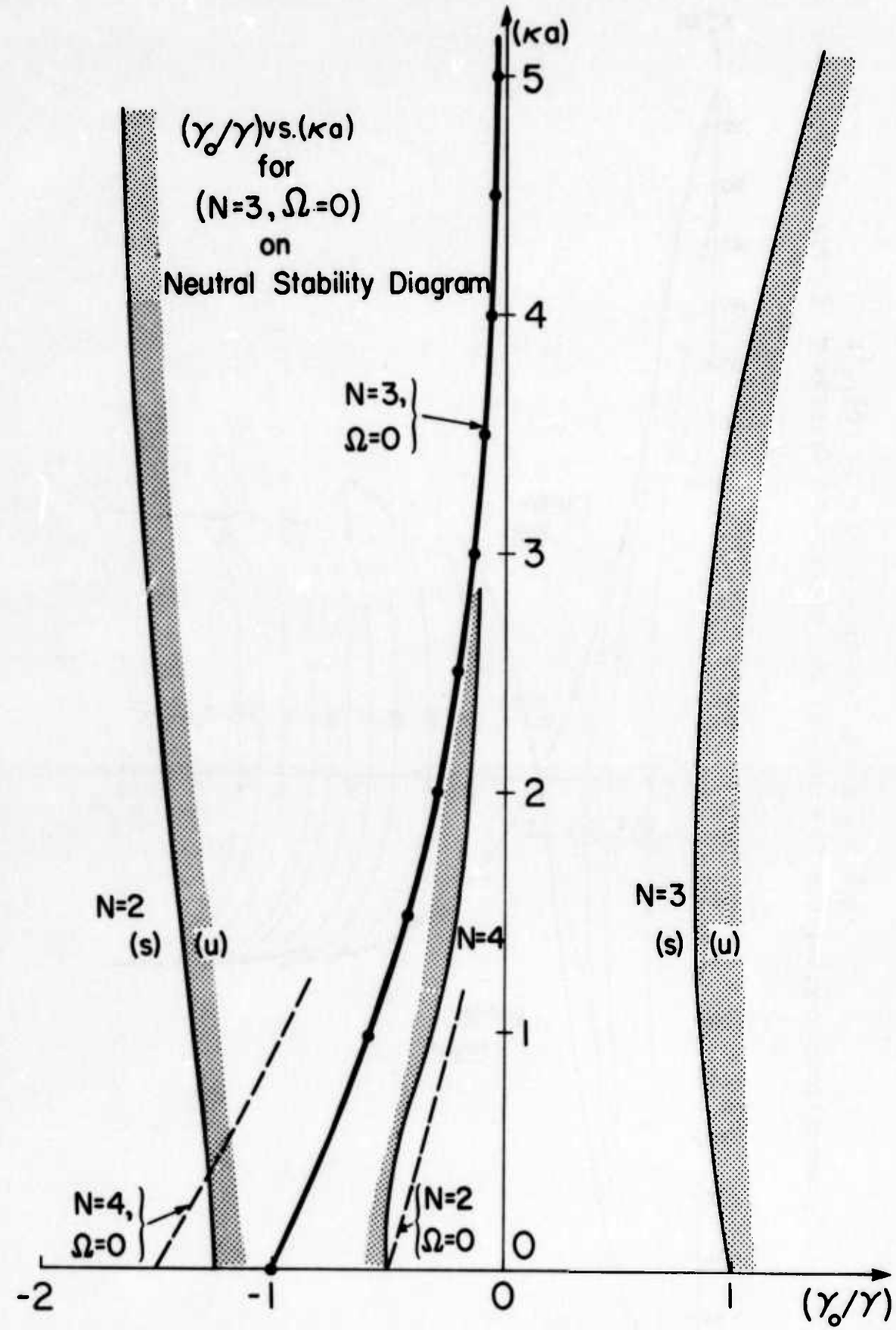

Fig. 2 γ_o vs. κ for $\Omega = 0$ and $N = 2, 3$ and 4; and Neutral Stability Curves for $N = 2, 3$ and 4.

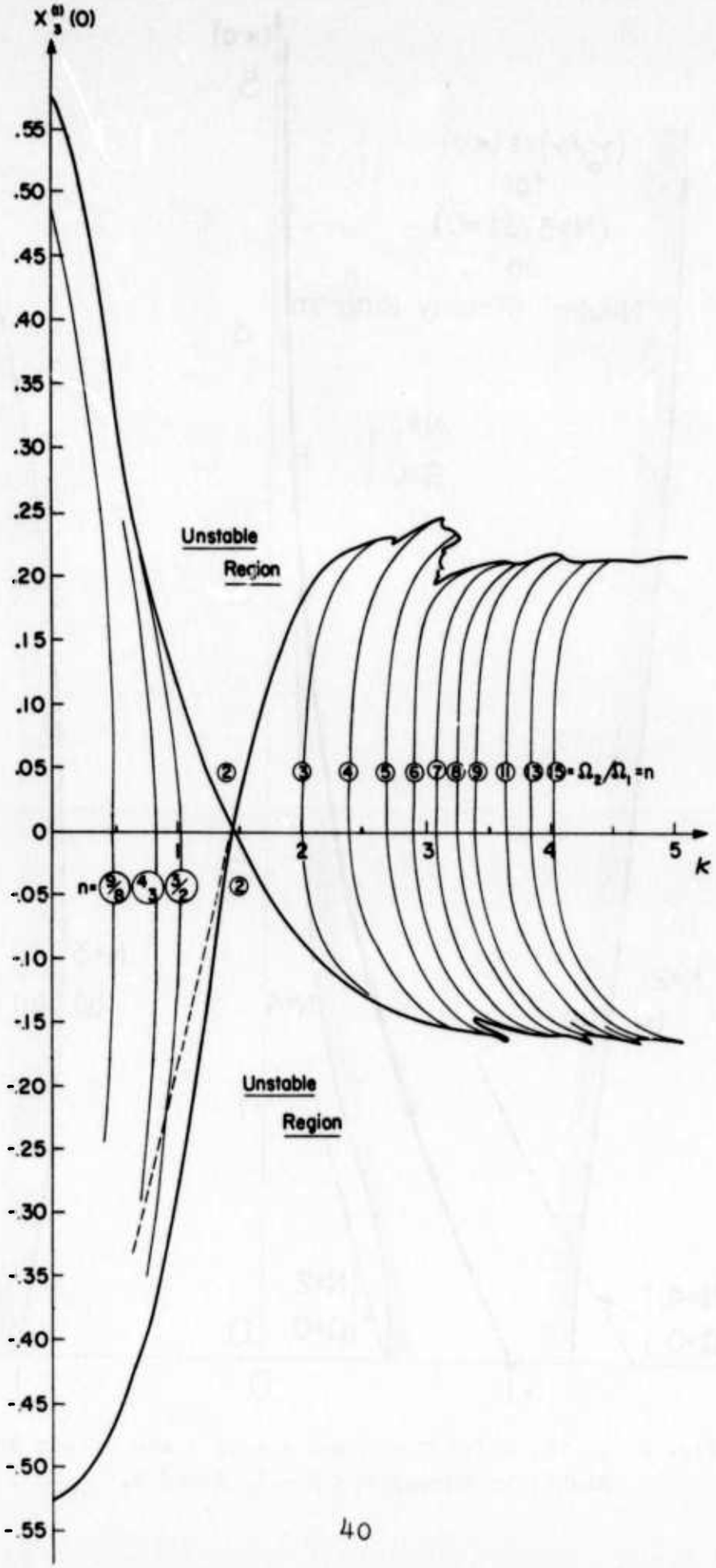

Fig. 3 Stability Boundaries for ($N=3;\Omega=0$) and Initial Displacement $x_3^{(1)}(0)$ of a Circle Vortex for $0 \leq \kappa \leq 5$.

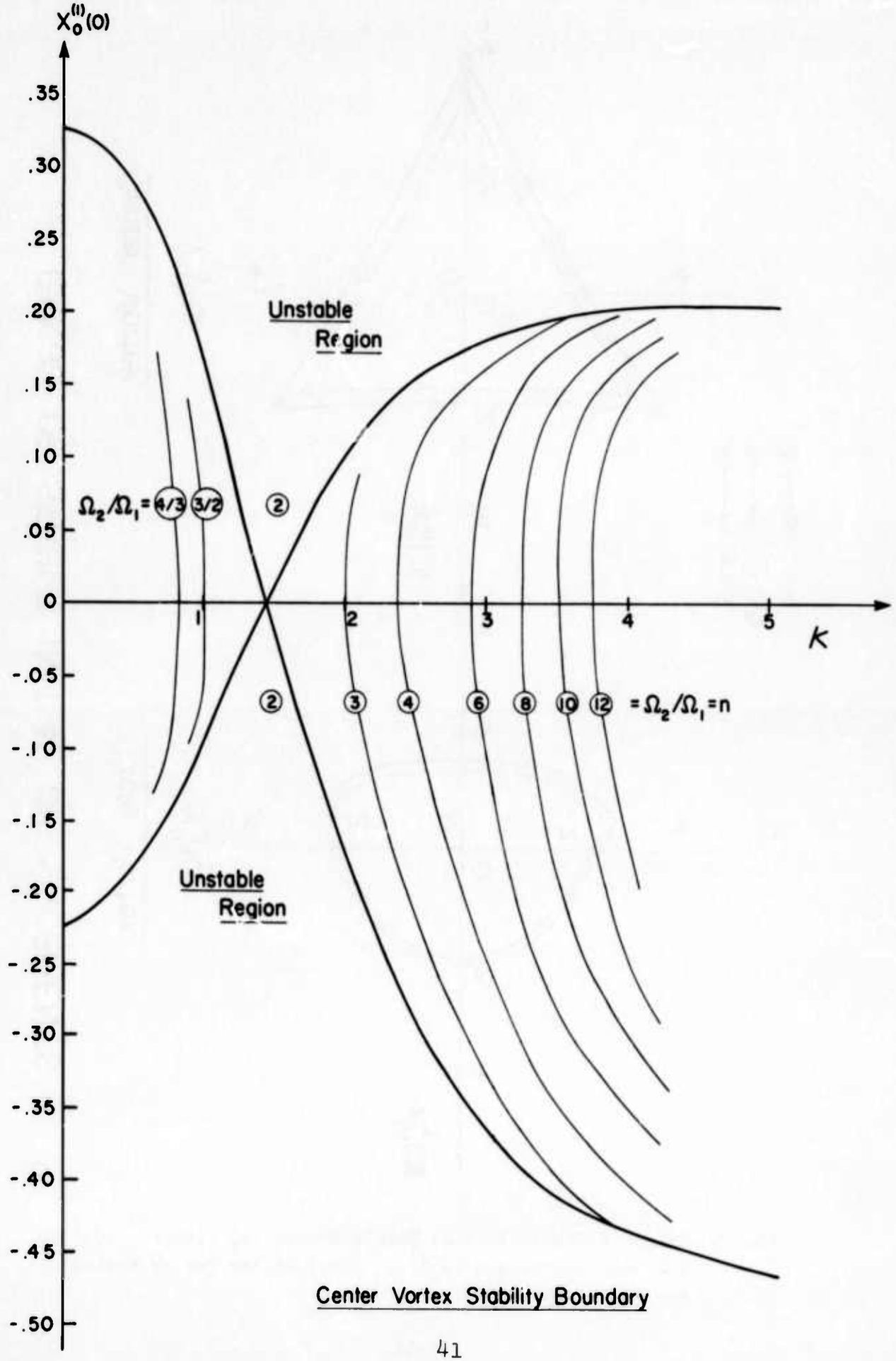

Fig. 4 Stability Boundaries for ($N = 3; \Omega = 0$) and Initial Displacement $x_0^{(1)}(0)$ of the Center Vortex for $0 \leq \kappa \leq 5$.

Fig. 5 Range of Stable Initial Displacements $[x_3^{(1)}(0), y_3^{(1)}(0)]$ of a Circle Vortex and $[x_0^{(1)}, y_0^{(1)}(0)]$ of the Center Vortex for $\kappa = 3$, 3.5 and 4.

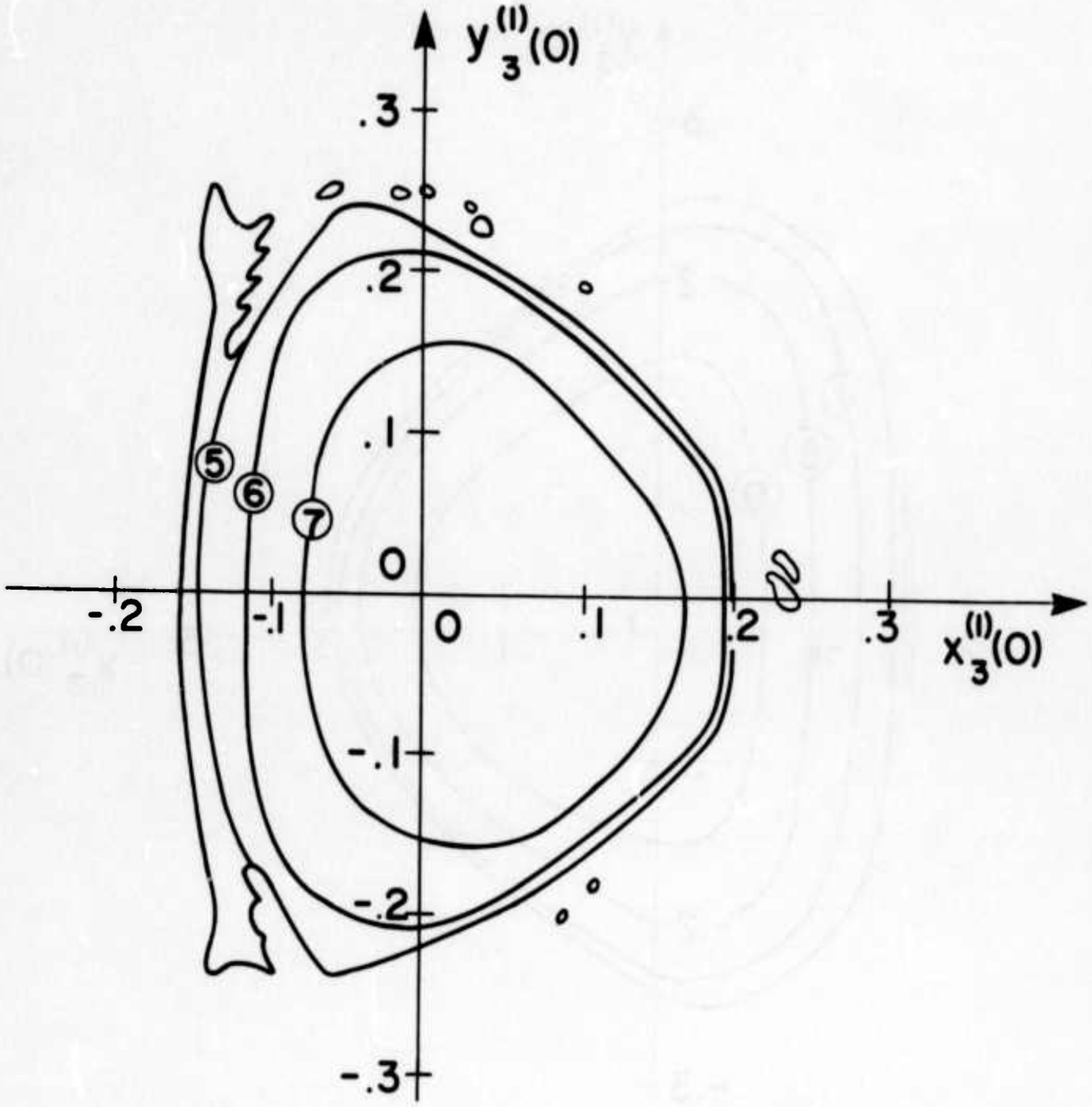

Fig. 6 Range of Stable Initial Displacements $[x_3^{(1)}(0), y_3^{(1)}(0)]$ of a Circle Vortex for $\kappa = 3.2$.

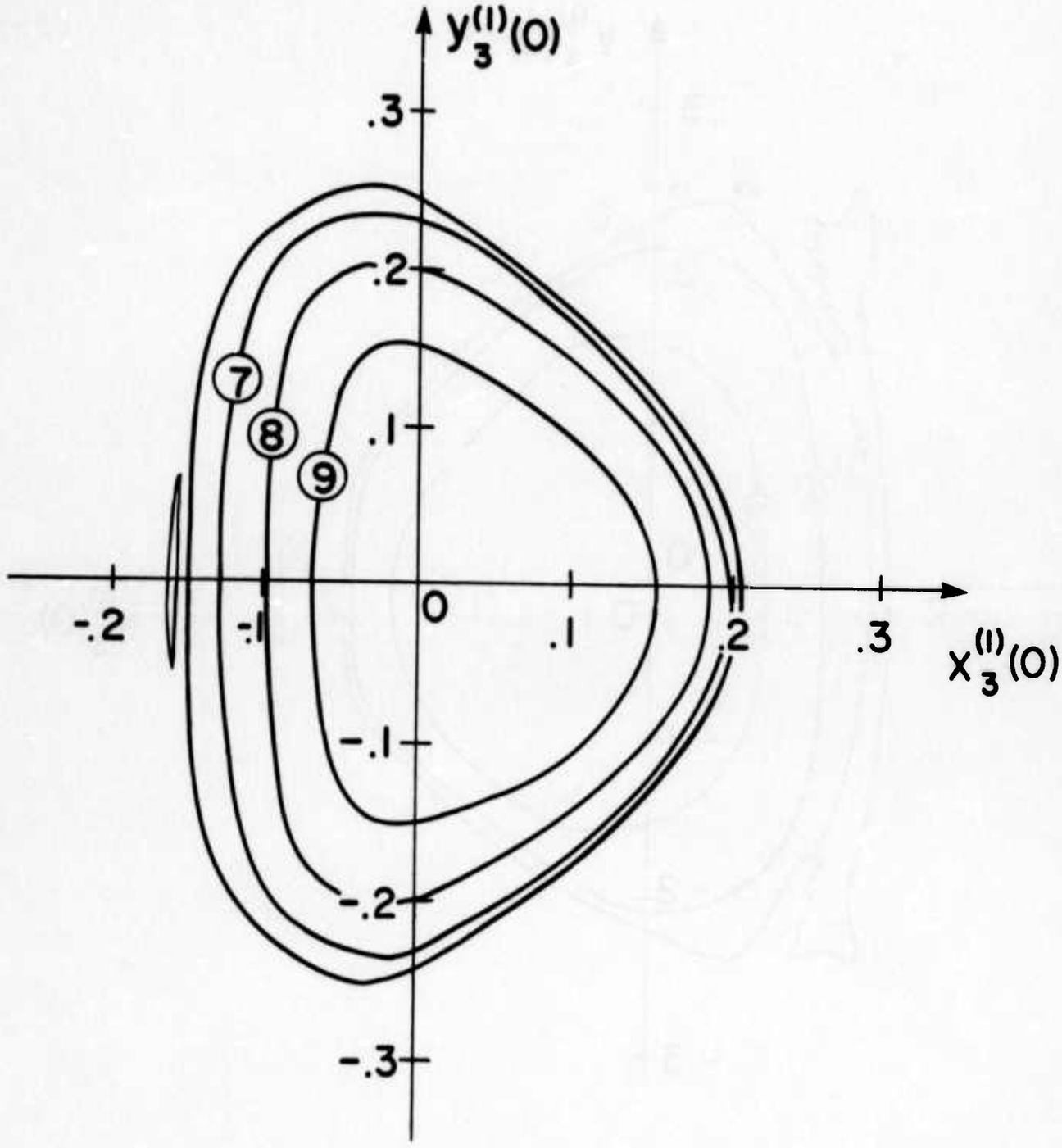

Fig. 7 Range of Stable Initial Displacements $[x_3^{(1)}(0), y_3^{(1)}(0)]$ of a Circle Vortex for $\kappa = 3.5$.

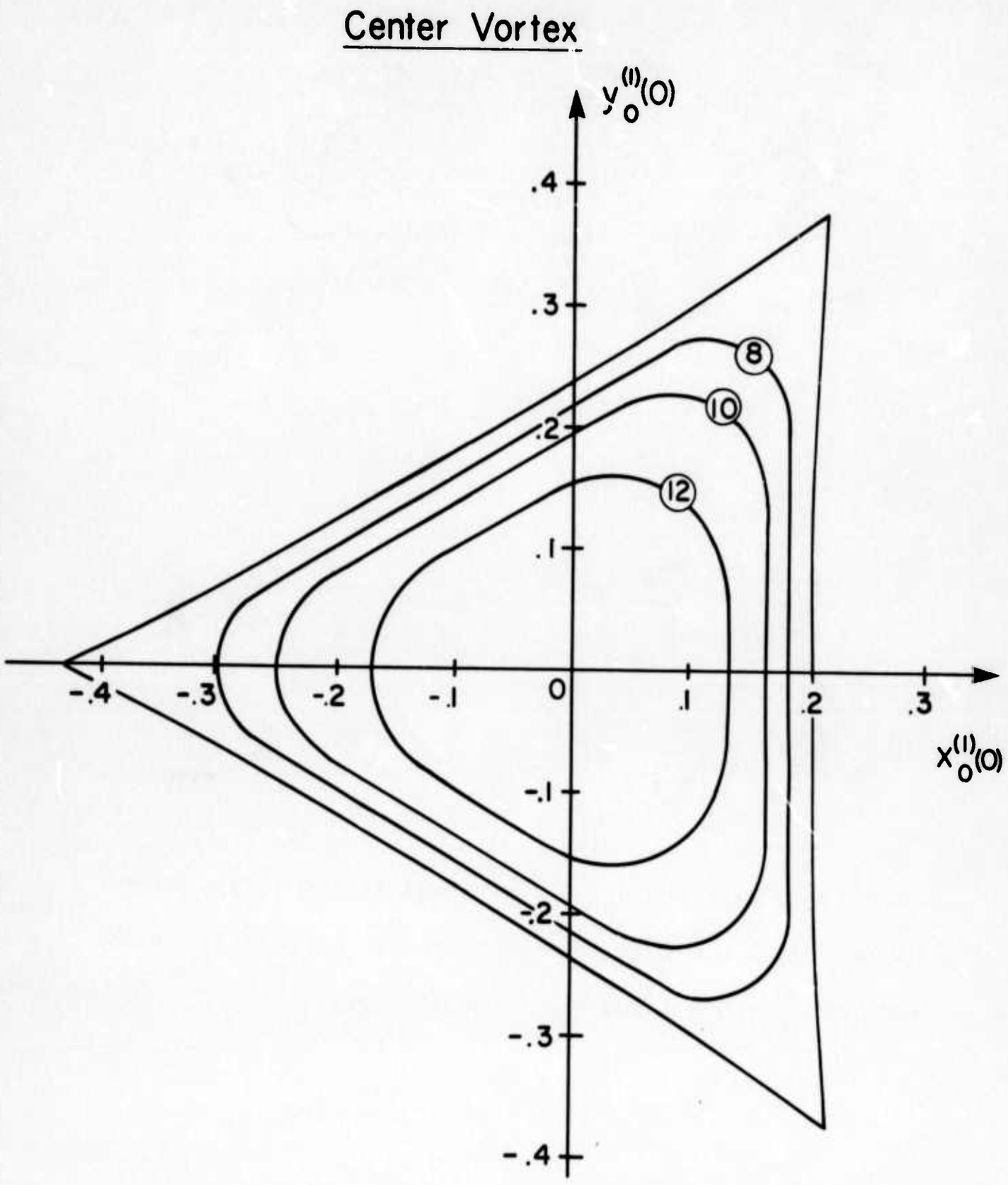

Fig. 8 Range of Stable Initial Displacements $[x_o^{(1)}(0), y_o^{(1)}(0)]$ of the Center Vortex for $\kappa = 4$.

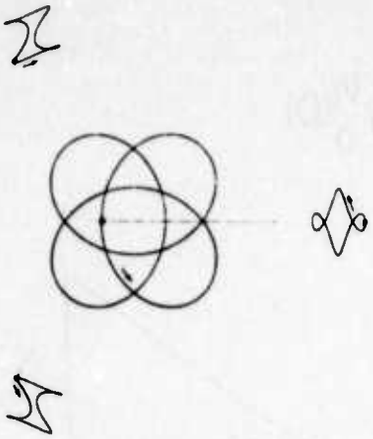

Fig. 9a

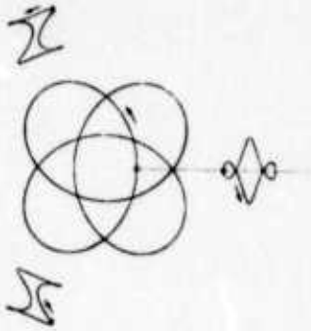

Fig. 9b

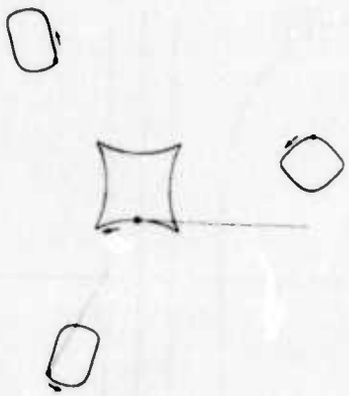

Fig. 9c

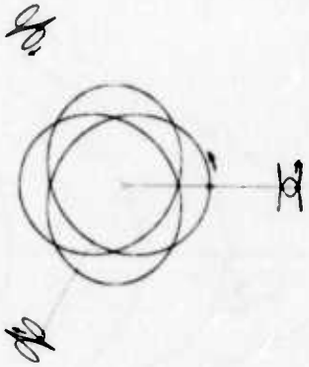

Fig. 9d

Vortex Trajectories for $\kappa = 2$ and Small Initial Displacements: (a) $x_3^{(1)}(0) = 0.001$, (b) $x_3^{(1)}(0) = -0.001$, (c) $y_3^{(1)}(0) = 0.001$ and (d) $x_0^{(1)}(0) = 0.001$; Magnification 500X.

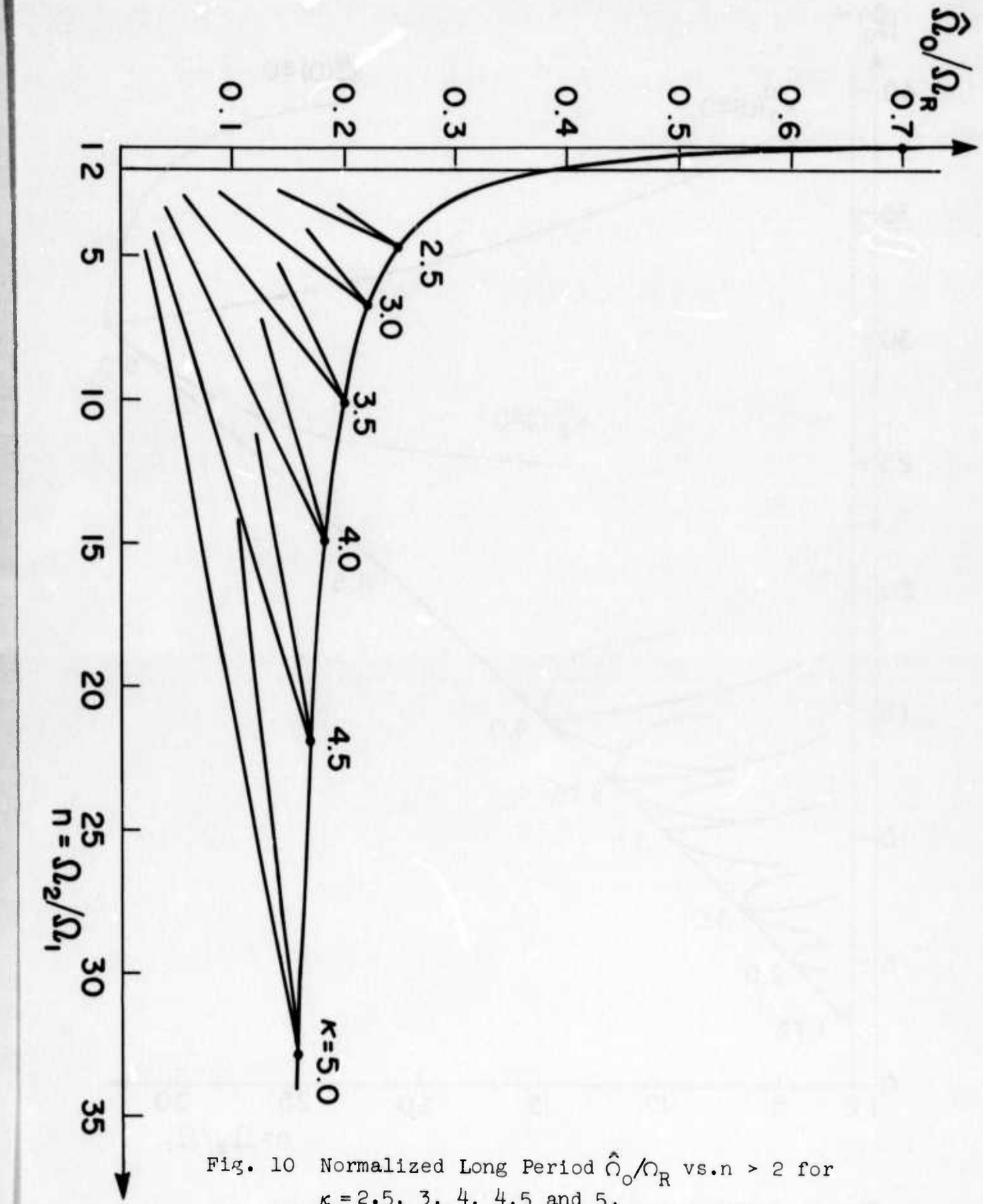

Fig. 10 Normalized Long Period $\hat{\Omega}_o/\Omega_R$ vs.n > 2 for $\kappa = 2.5$, 3, 4, 4,5 and 5.

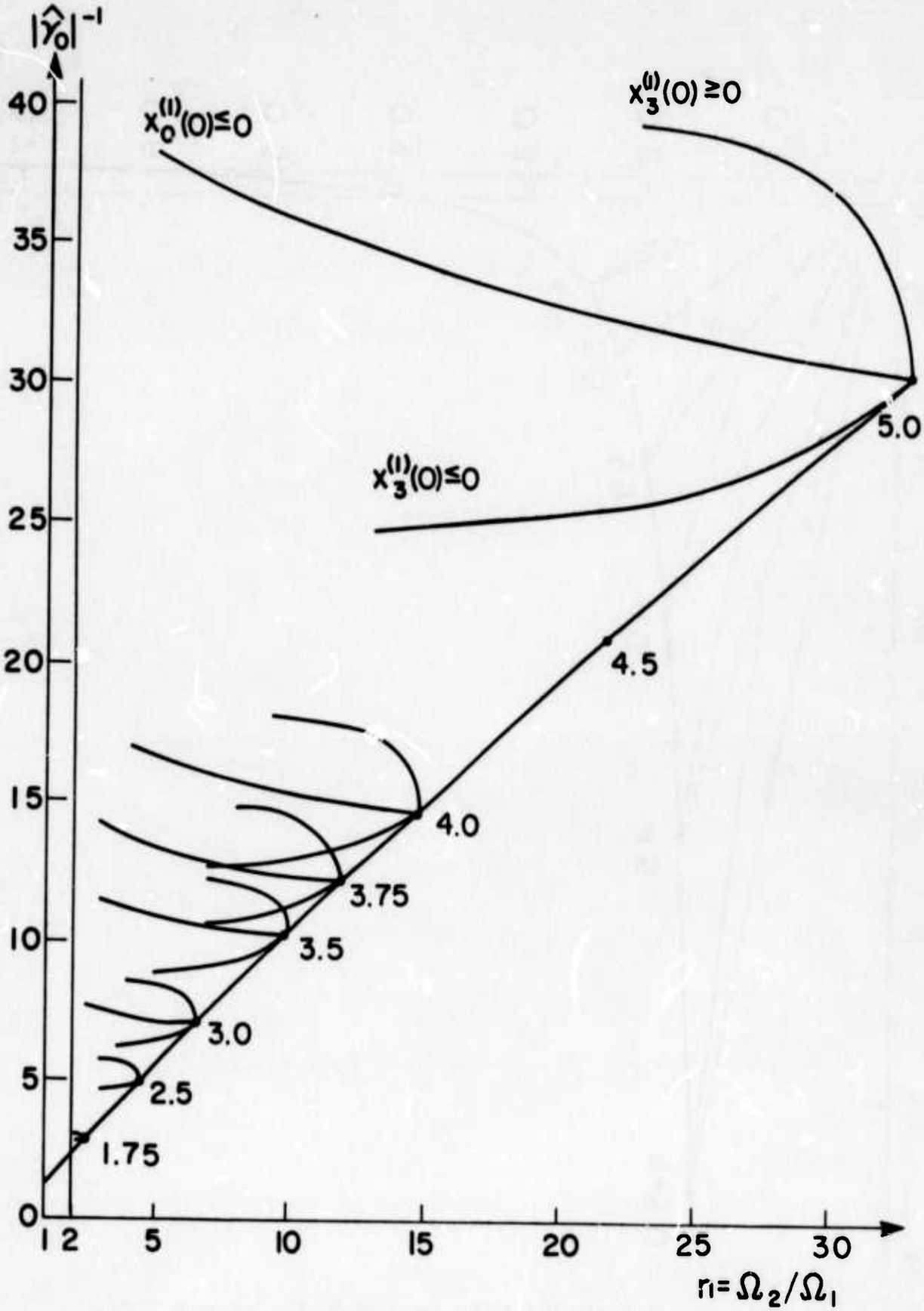

Fig. 11 Vortex Strength Ratio $|\hat{\gamma}_0|^{-1}$ vs. $n > 2$ for $\kappa = 1.75$, 2.5, 3, 3.5, 3.75, 4 and 5.

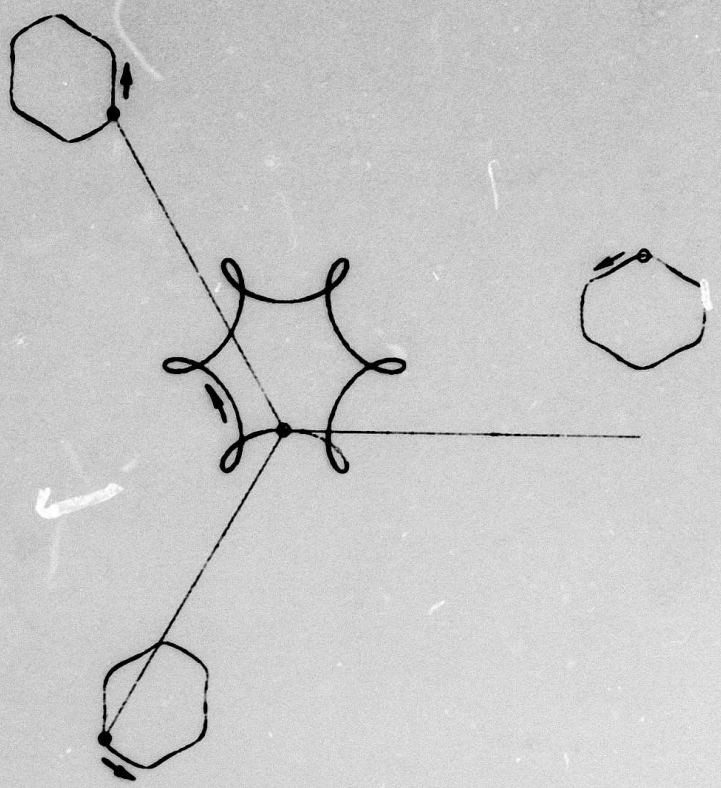

Fig. 12

Vortex Trajectories for $[\kappa, n; x_3^{(1)}(0), y_3^{(1)}(0)] = (2.66, 5; 0, 0.001)$.

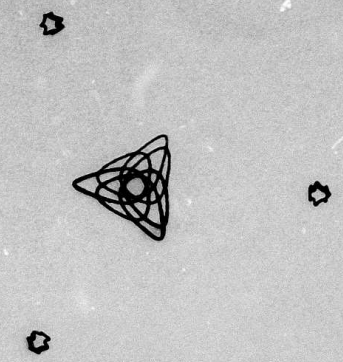

Fig. 13a

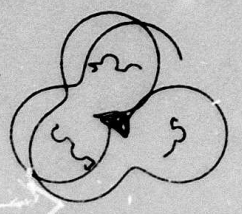

Fig. 13b

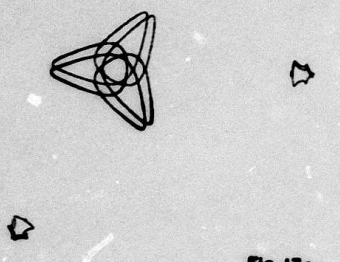

Fig. 13c

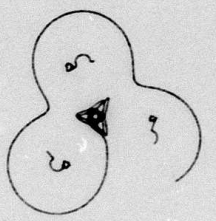

Fig. 13d

Vortex Trajectories for:

(a) $[\kappa, n; x_3^{(1)}(0), y_3^{(1)}(0)] = (3.2, 6; 0.196, 0)$;

(b) $\kappa = 3.2$ with $[x_3^{(1)}(0), y_3^{(1)}(0)] = (0.215, 0)$, unstable;

(c) $[\kappa, n; x_3^{(1)}(0), y_3^{(1)}(0)] = (3.2, 5; 0.230, 0)$; and

(d) $\kappa = 3.2$ with $[x_3^{(1)}(0), y_3^{(1)}(0)] = (0.240, 0)$, unstable.

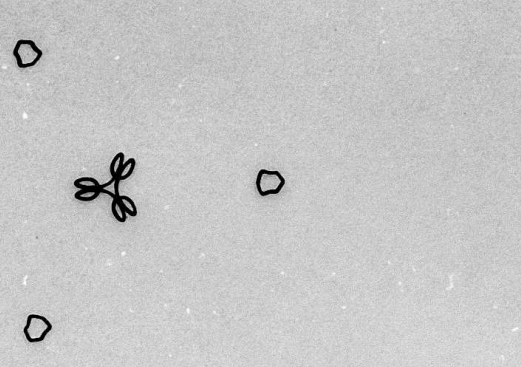

Fig. 14a

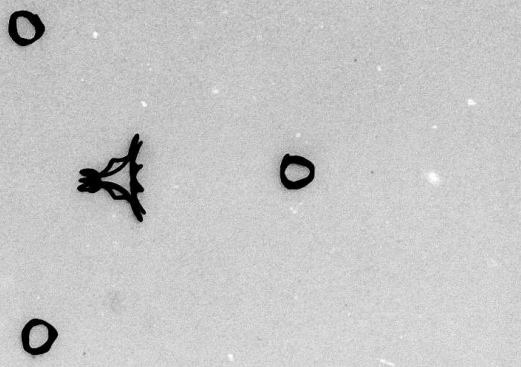

Fig. 14b

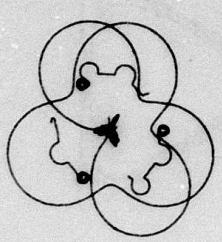

Fig. 14c

Vortex Trajectories for:

(a) $[\kappa, n; x_3^{(1)}(0), y_3^{(1)}(0)] = (3.2, 5; -0.120, 0.208)$;

(b) $[\kappa, n; x_3^{(1)}(0), y_3^{(1)}(0)] = (3.2, 9/2; -0.130, 0.240)$; and

(c) $\kappa = 3.2$ with $[x_3^{(1)}(0), y_3^{(1)}(0)] = (-0.120, 0.235)$, unstable.

The second order drift corrections are: (a) 8.4%; (b) 10.4%; (c) 10%.

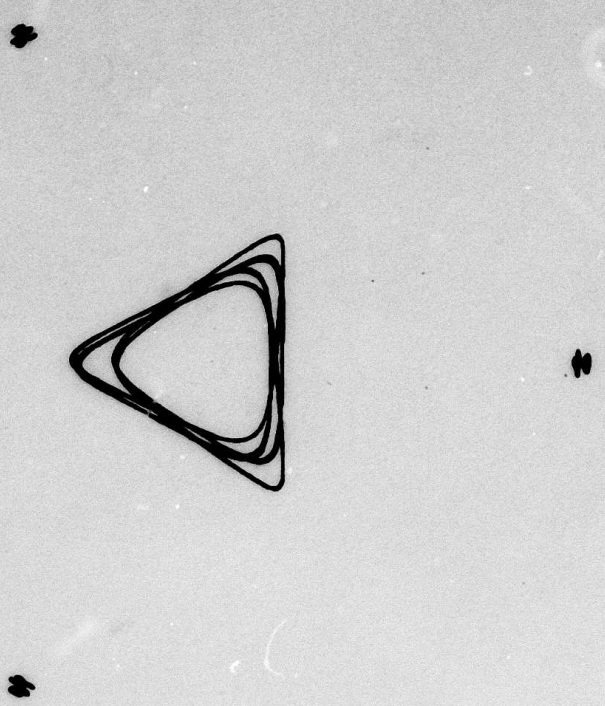

Fig. 15

Vortex Trajectories for $[\kappa, n; x_o^{(1)}(0), y_o^{(1)}(0)] = (3.5, 4; 0.1955, 0)$; -11.1%.

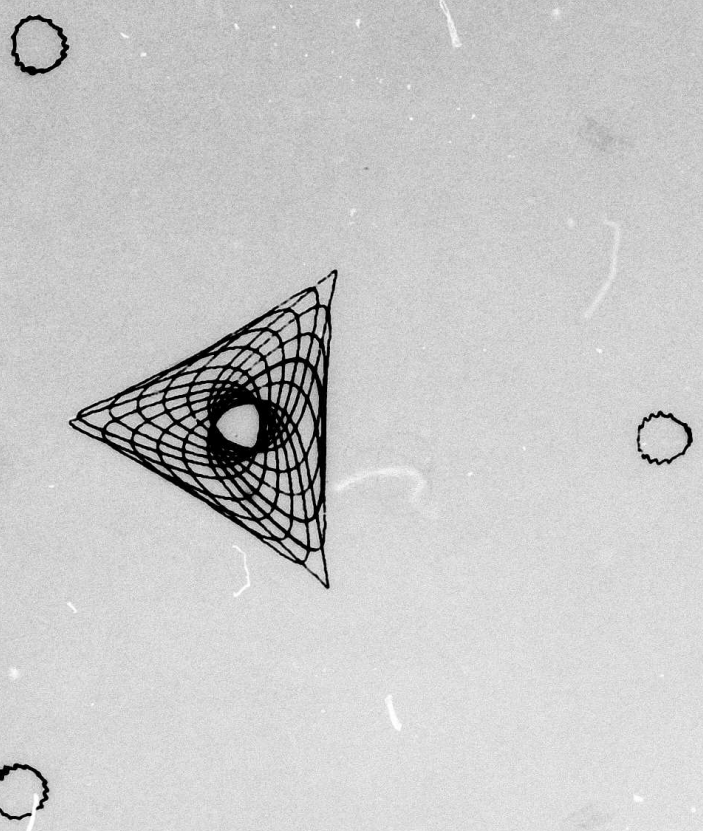

Fig. 16

Vortex Trajectories for $[\kappa, n; x_3^{(1)}(0), y_3^{(1)}(0)] = (4.5, 15; 0.2138, 0)$.

Fig. 17

Vortex Trajectories for $[\kappa, n; x_3^{(1)}(0), y_3^{(1)}(0)] = (1.25, 2; -0.118, 0)$.

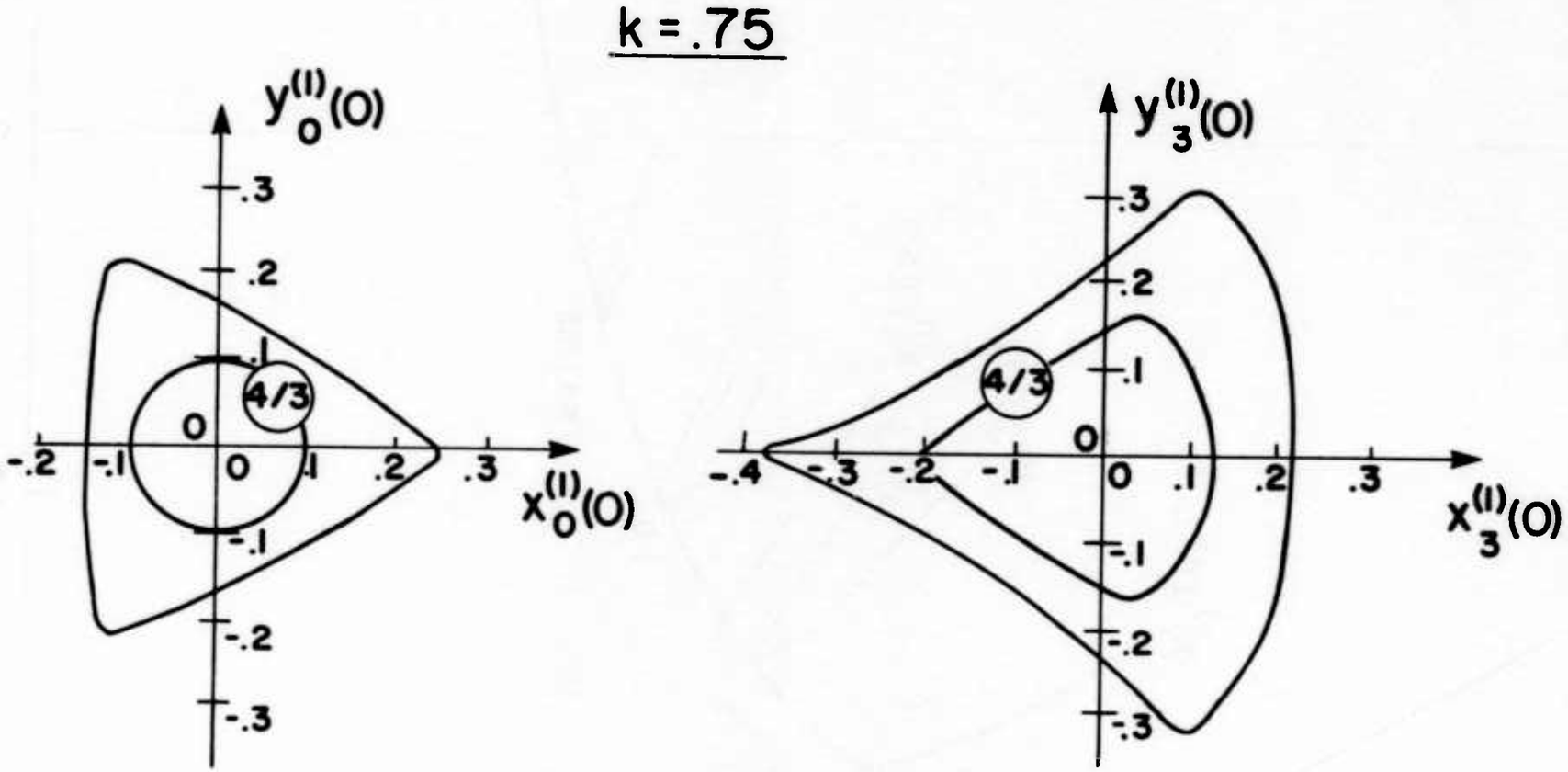

Fig. 18 Range of Stable Initial Displacements $[x_3^{(1)}(0), y_3^{(1)}(0)]$ of a Circle Vortex and $[x_0^{(1)}(0), y_0^{(1)}(0)]$ of the Center Vortex for $\kappa = 0.75$.

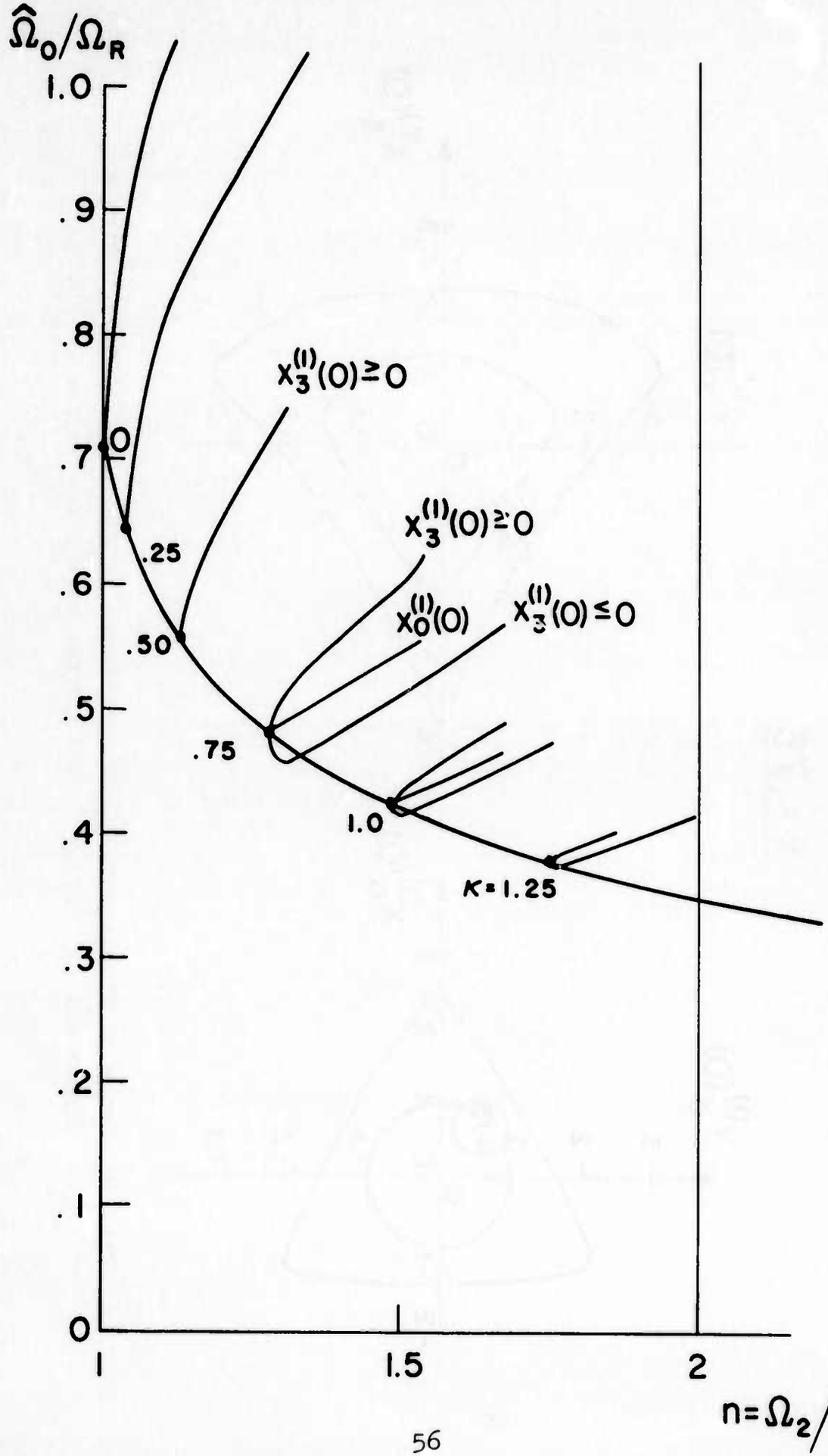

Fig. 19 Normalized Long Period $\hat{\Omega}_o/\Omega_R$ vs. $n < 2$ for $\kappa = 0$, 0.25, 0.50, 0.75, 1.0 and 1.25.

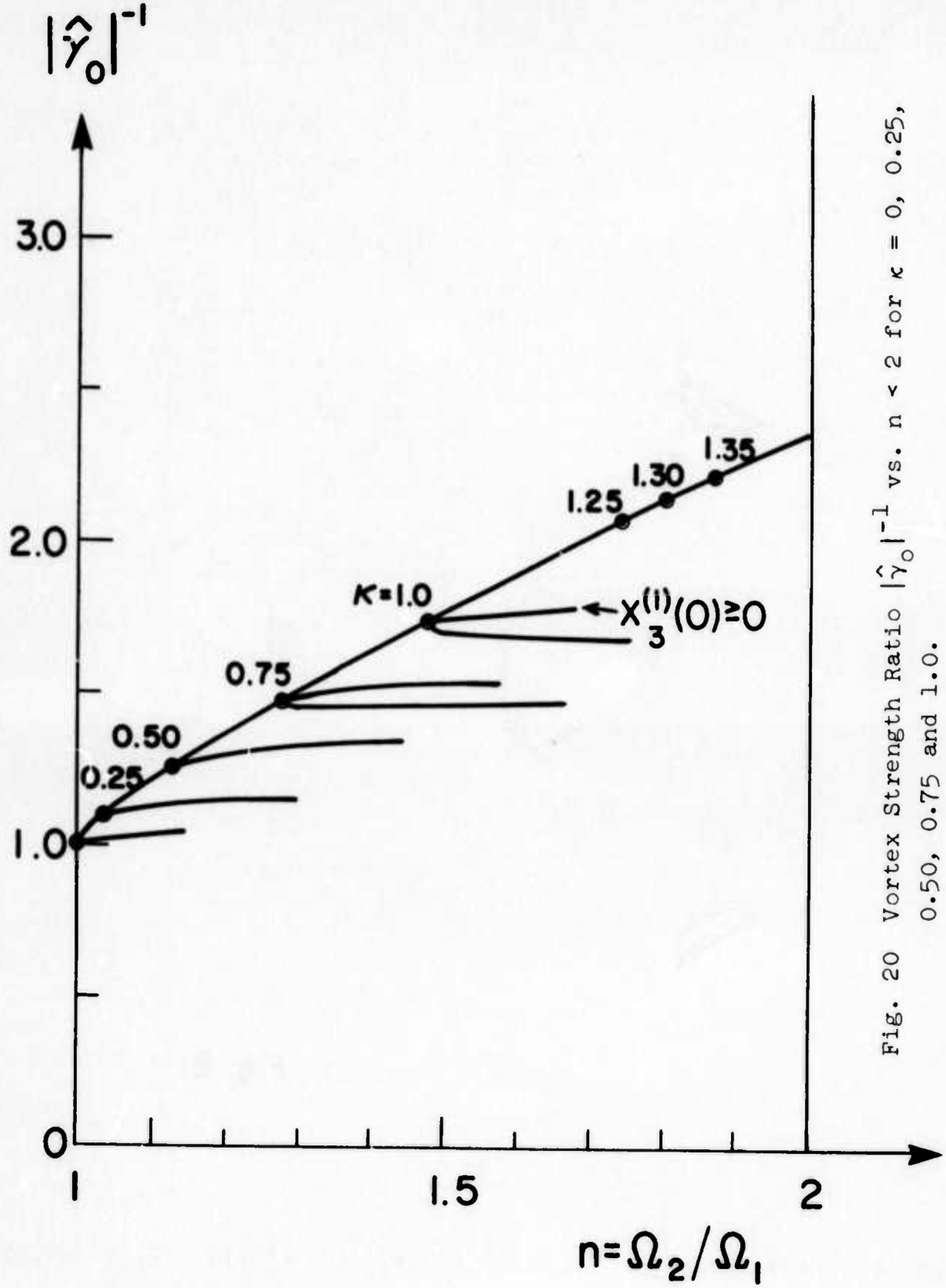

Fig. 20 Vortex Strength Ratio $|\hat{\gamma}_0|^{-1}$ vs. $n < 2$ for $\kappa = 0$, 0.25, 0.50, 0.75 and 1.0.

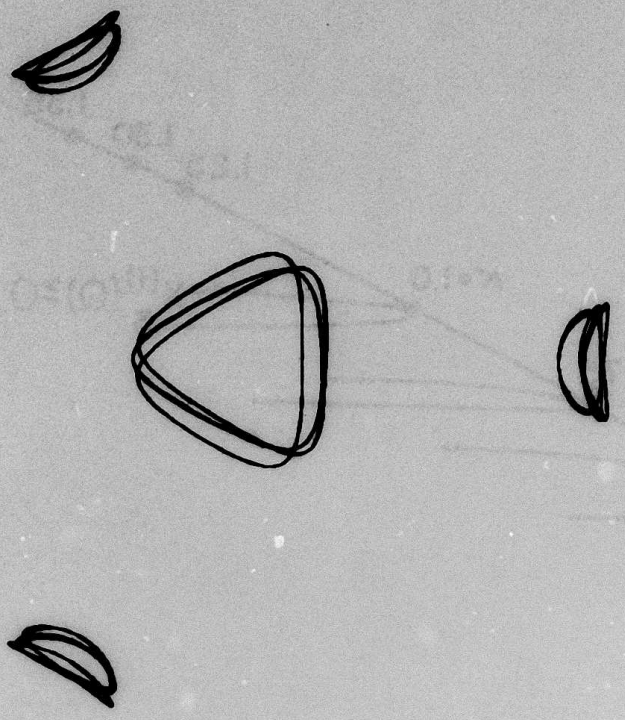

Fig. 21

Vortex Trajectories for $[\kappa, n; x_3^{(1)}(0), y_3^{(1)}(0) = (0.75, 3/2; -0.350, 0)$.

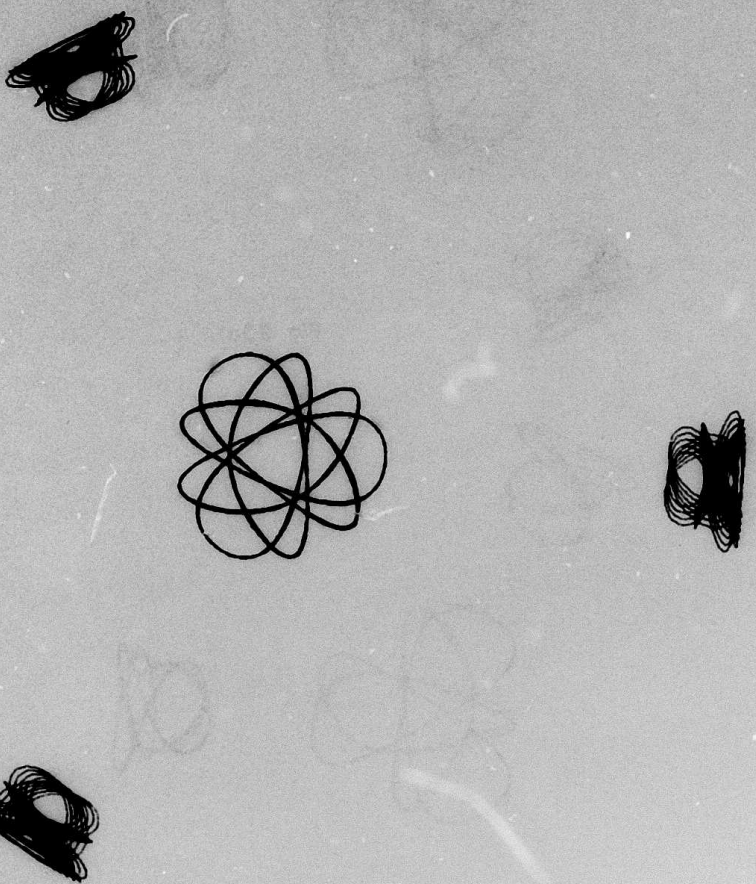

Fig. 22

Vortex Trajectories for $[\kappa, n; x_3^{(1)}(0), y_3^{(1)}(0)] = (0.5, 5/4; 0.264, 0)$.

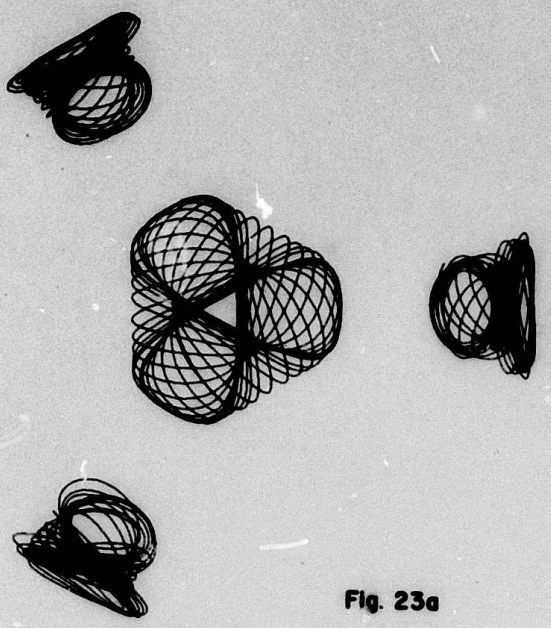

Fig. 23a

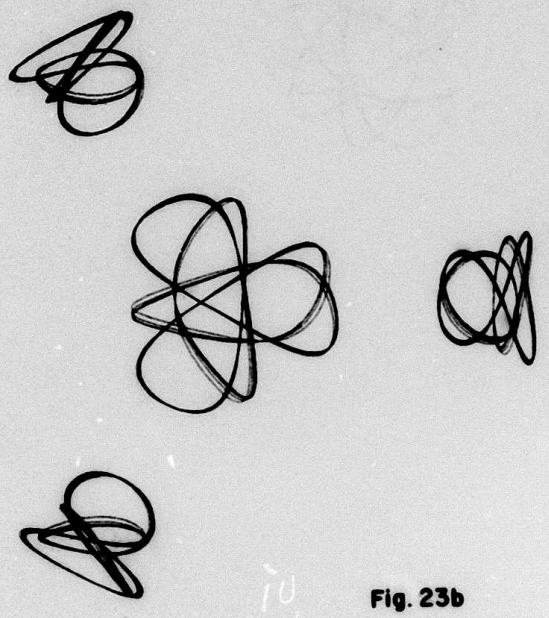

Fig. 23b

(a) Vortex Trajectories for $[\kappa, n; x_3^{(1)}(0), y_3^{(1)}(0)]$ $= (0.25, 25/19; 0.452, 0)$.

(b) Vortex Trajectories for $[\kappa, n; x_3^{(1)}(0), y_3^{(1)}(0)]$ $= (0.25, 4/3; 0.456, 0)$.

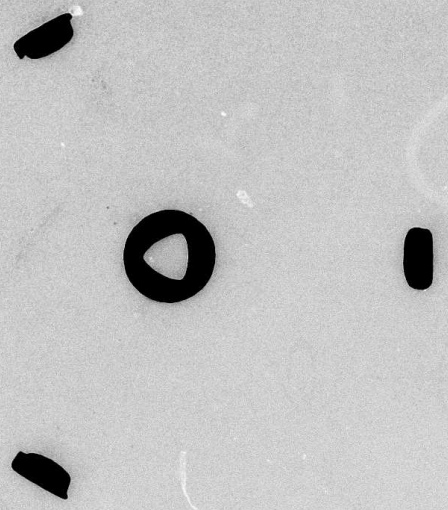

Fig. 24a

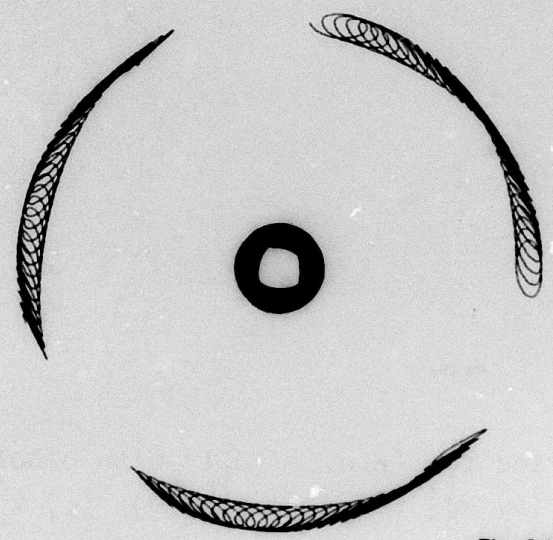

Fig. 24b

(a) $[\kappa, n; x_3^{(1)}(0), y_3^{(1)}(0)] = (0.125, 27/26; 0.250, 0)$;
with -1.15% second order drift correction;

(b) $\kappa = 0.125$ and $[x_3^{(1)}(0), y_3^{(1)}(0)] = (0.250, 0)$,
without second order drift correction.

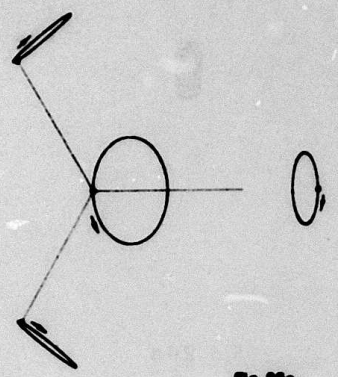

Fig. 23a

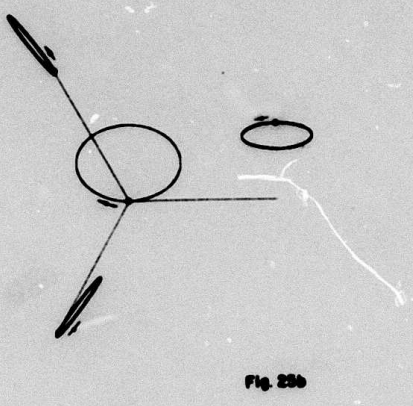

Fig. 23b

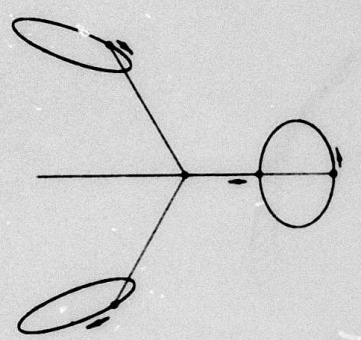

Fig. 23c

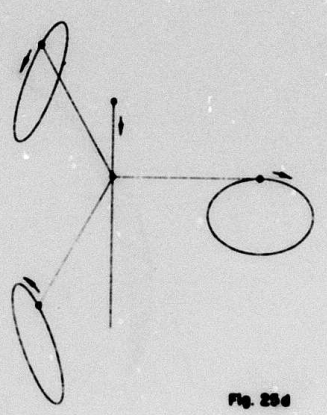

Fig. 23d

Vortex Trajectories for $(\kappa,n) = (0,1)$ with 0.001 Initial Displacements: (a) $x_3^{(1)}(0)$, (b) $y_3^{(1)}(0)$, (c) $x_0^{(1)}(0)$ and (d) $y_0^{(1)}(0)$; Magnification 500X.

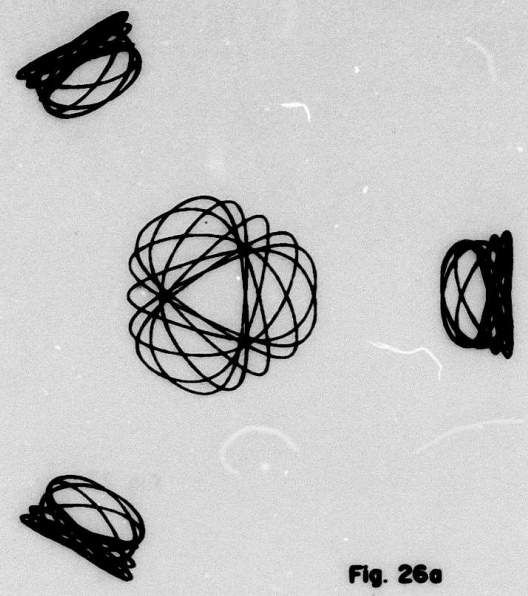

Fig. 26a

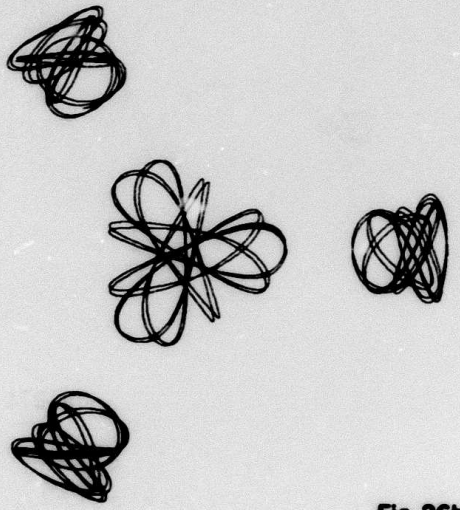

Fig. 26b

(a) Vortex Trajectories for $[\kappa, n; x_3^{(1)}(0), y_3^{(1)}(0)] = (0, 8/7; 0.503, 0)$.

(b) Vortex Trajectories for $[\kappa, n; x_o^{(1)}(0), y_o^{(1)}(0)] = (0, 6/5; 0.300, 0)$.

Fig. 27a

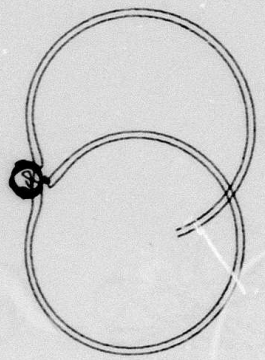

Fig. 27b

(a) Vortex Trajectories for $\kappa = 0$ and $[x_o^{(1)}(0), y_o^{(1)}(0)] = (-0.300, 0)$; $\gamma_o = -1$; no drift correction; absolutely unstable.

(b) Vortex Trajectories for $\kappa = 0$ and $[x_3^{(1)}(0), y_3^{(1)}(0)] = (0.600, 0)$; $\hat{\gamma}_o = -0.93500$; unstable.

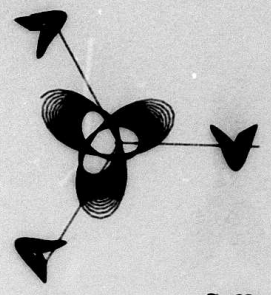

Fig. 28a

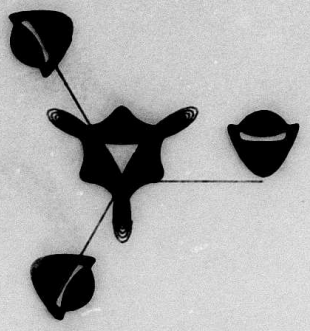

Fig. 28b

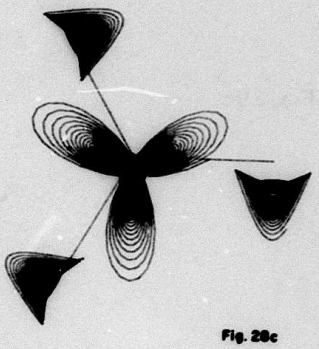

Fig. 28c

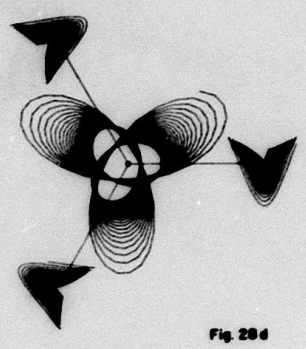

Fig. 28d

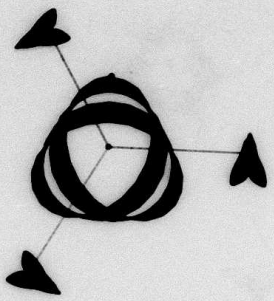

Fig. 28e

Vortex Trajectories for $\kappa = 1.4476$ and Initial Displacements:
(a) $x_3^{(1)}(0) = -0.005$, (b) $y_3^{(1)}(0) = 0.005$, (c) $y_3^{(1)}(0) = -0.005$,
(d) $x_o^{(1)}(0) = 0.005$ and (e) $y_o^{(1)}(0) = 0.005$.
The scale factors are 50, 100, 50, 50, 100.

Fig. 29a

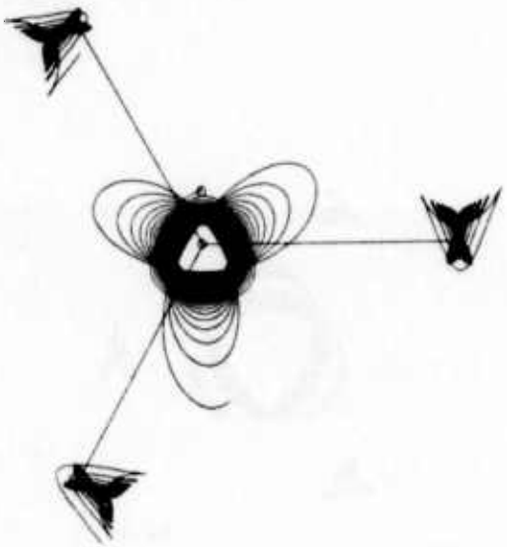

Fig. 29b

Vortex Trajectories for $\kappa = 1.4476$ and Initial Displacements:
(a) $y_o^{(1)}(0) = 0.015$ and (b) $y_o^{(1)}(0) = 0.02$.
Scales are 50X and 10X.

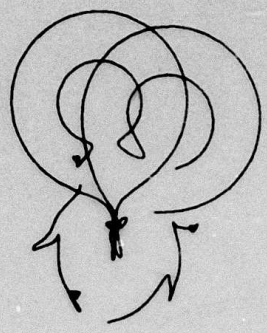

Fig. 30a

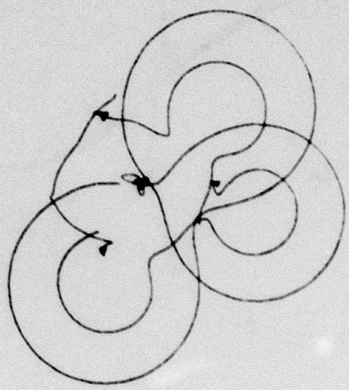

Fig. 30b

Unstable Vortex Trajectories for $\kappa = 1.4476$ and Initial Displacements: (a) $[x_o^{(1)}(0), y_o^{(1)}(0)] = (0.01, 0.03)$ and (b) $[x_o^{(1)}(0), y_o^{(1)}(0)] = (-0.01, 0.03)$.

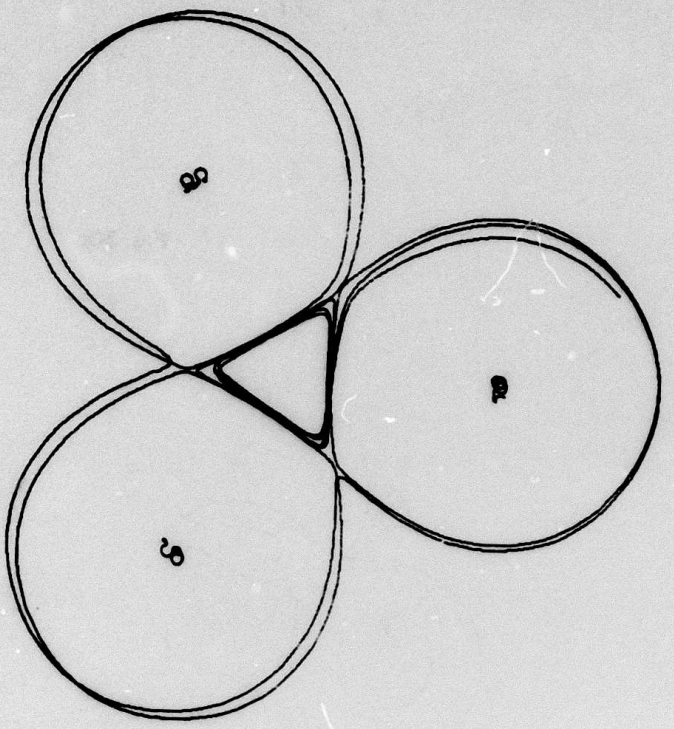

Fig. 31

Unstable Vortex Trajectories for $\kappa = 5$ and $[x_o^{(1)}(0), y_o^{(1)}(0)] = (0{\cdot}210, 0)$.

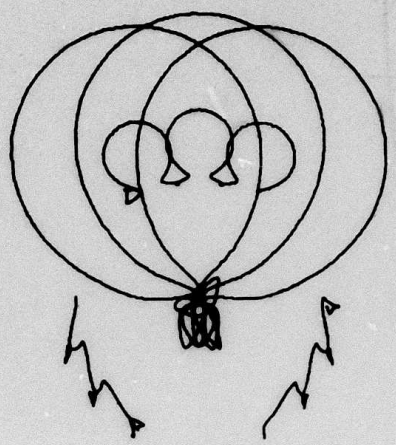

Fig. 32

Unstable Vortex Trajectories for $\kappa = 2.5$ and $[x_3^{(1)}(0), y_3^{(1)}(0)] = (-0.130, 0)$.

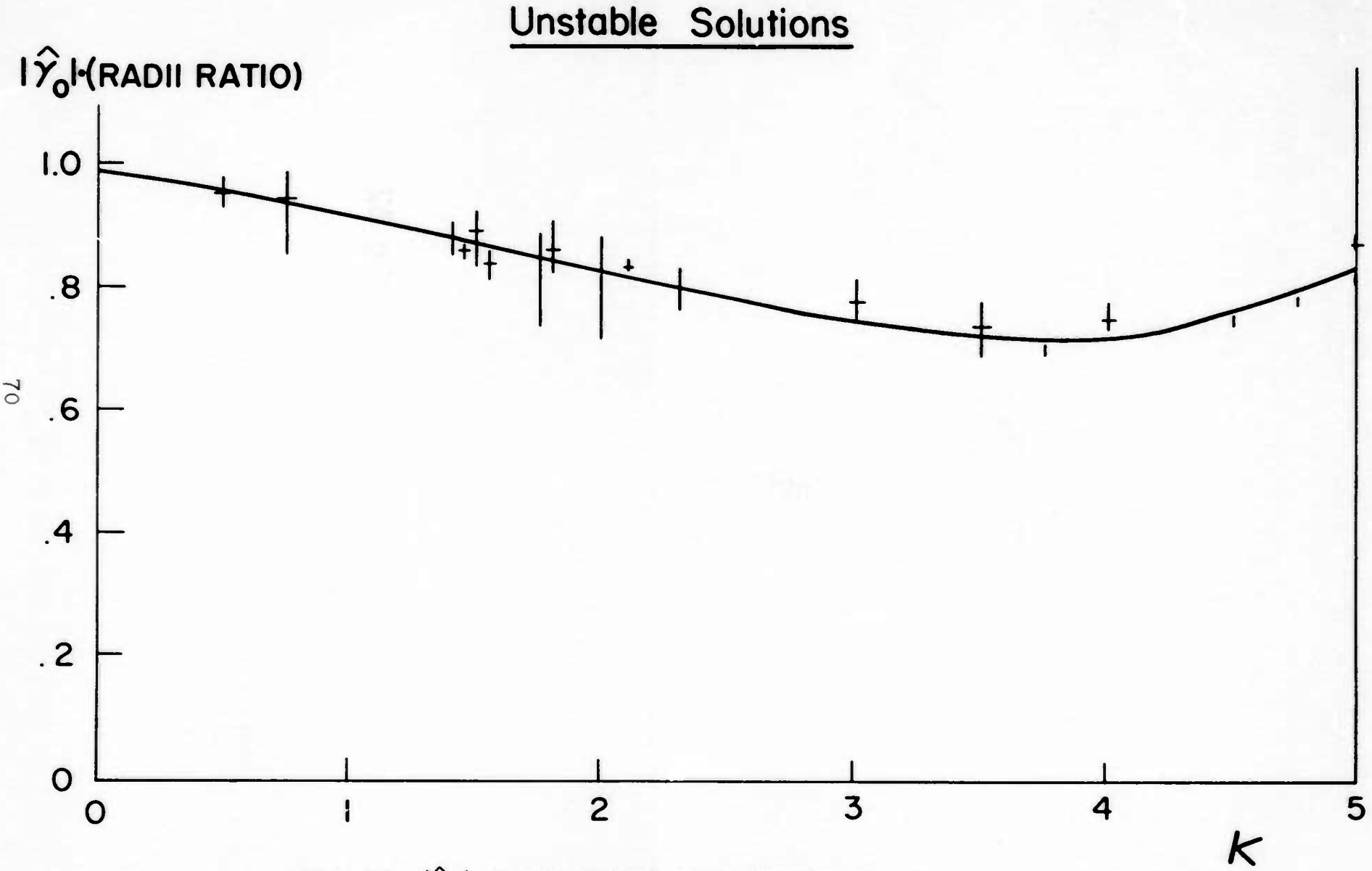

Fig. 33 $|\hat{\gamma}_0|$·(Radii Ratio) vs. κ for $0 \leq \kappa \leq 5$.